

## New data on the $K\bar{K}$ threshold region and the nature of the $f_0(S^*)$

D. Morgan

*Rutherford Appleton Laboratory, Chilton, Didcot, Oxon, OX11 0QX, United Kingdom*

M. R. Pennington

*Centre for Particle Theory, University of Durham, Durham, DH1 3LE, United Kingdom*

(Received 8 January 1993)

We combine new data on  $f_0(S^*)$  production in  $J/\psi$  and  $D_s$  decays with earlier information on central production and elastic  $\pi\pi$ ,  $K\bar{K}$  processes to make a fresh examination of the  $f_0(S^*)$  resonance. The key feature of our amplitude analysis is its strict enforcement of unitarity. This allows the good energy resolution of the new  $J/\psi \rightarrow \phi\pi\pi(K\bar{K})$  data to play its full role in delineating the  $f_0(S^*)$  resonance structure that experiment demands. This enables us to distinguish alternative resonance mechanisms that have been proposed: we conclude that  $f_0(S^*)$  is most probably not a  $K\bar{K}$  molecule, nor an amalgam of two resonances, but a conventional Breit-Wigner-like structure. In this preferred description, the  $f_0(S^*)$  has rather a narrow width ( $\Gamma_0 \sim 52$  MeV) and comparable couplings to  $\pi\pi$  and  $K\bar{K}$ . Possible spectroscopic interpretations are considered.

PACS number(s): 14.40.Cs, 13.20.Fc, 13.20.Gd, 13.25.+m

### I. INTRODUCTION

Low mass meson interactions play a fundamental role in the study of hadron physics at the Fermi scale. Not only are mesonic channels,  $\pi\pi$ ,  $K\bar{K}$ , etc., the most abundant outcome of production processes and decays, but it is their exchanges that control the bulk of nuclear binding. While one-pion exchange is, of course, responsible for the longest range force, the next in strength is two-pion exchange with  $I=J=0$ . Despite its importance, the nature of the isoscalar scalar interaction is still unclear. The states that occur in this channel have been variously ascribed [1] as conventional  $q\bar{q}$  mesons [2], multiquark states [3],  $K\bar{K}$  molecules [4], glueballs [5], and/or hybrids [6]. The aim of this paper is to extend previous analyses by incorporating the latest experimental information and to focus on these issues of the nature of possible resonant states by concentrating on the crucial  $K\bar{K}$  threshold region.

Below 1100 MeV it has long been known that essentially the only contributions with  $I=J=0$  quantum numbers come from  $\pi\pi$  and  $K\bar{K}$  final states and that other channels with more pions add less than a few percent to the integrated cross sections [7], and so can be safely neglected, as we do weak and electromagnetic contributions. The most extensive analysis to date of all high statistics data with  $\pi\pi$  and  $K\bar{K}$  final states is by the Au-Morgan-Pennington (AMP) collaboration [8]. An unexpected outcome of this analysis was the conclusion that the  $f_0(S^*)$  most likely comprised two resonances—a fairly narrow object coupling to  $\pi\pi$  and  $K\bar{K}$  and a very narrow  $K\bar{K}$  bound state coupling weakly to the  $\pi\pi$  channel; all this on a background furnished by a very broad  $f_0(\epsilon(1000))$ . The interpretation of these results in terms of quark model states is quite nontrivial in a channel with the quantum numbers of the vacuum; consequently,

which are members of the expected  $L=S=1$   $q\bar{q}$   $0^{++}$  multiplet is far from unambiguously established [9].

Crucial new information, particularly on  $J/\psi$  decays, has become available and that is our principal reason for returning to this problem. A parallel development has been the emergence of a new orthodoxy for spectroscopic assignments of the scalars [10]. A key ingredient of this scheme is a  $K\bar{K}$  molecular composition for the  $f_0(S^*)$  [and  $a_0(\delta)$ ] [4]. In suitable circumstances, this hypothesis can be tested [11,12], as we describe.

The method adopted is to focus on the resonance pole topology that the data require for the  $f_0(S^*)$ . It is in terms of this that we distinguish alternative compositions for this state. The issue is exemplified by the question of whether the deuteron is an elementary state of baryon number two or more legitimately thought of as a bound state of two nucleons [13]. Within a fully fledged dynamical discussion, e.g., via dispersion relations, this question is equivalent to asking whether or not the deuteron is a Castillejo-Dalitz-Dyson (CDD) pole [14]. In other words, is the deuteron characterized wholly as a scattering state of two nucleons or does its Fock space include a significant elementary component of six quarks? This Weinberg has answered [13]. Analogously, the picture of the  $S^*$  and  $\delta$  as  $K\bar{K}$  molecules presupposes that these resonances are characterized wholly as bound states of a kaon and antikaon and that there is no sizable admixture of  $q\bar{q}$  or  $qq\bar{q}\bar{q}$  or glue in their wave functions. This is the question we address.

To achieve this, one needs to study the energy dependence of scattering amplitudes as determined by experiment. Such amplitudes are “analytic” and one can continue them to complex values of the energy  $E$ . As is well known, unstable particles correspond to poles in the complex  $E$  plane below the real axis [15]. The existence of thresholds in scattering processes imposes a *sheet struc-*

ture on the continued scattering amplitudes. This sheet structure arises because the functional form of the scattering amplitude, in fact, depends upon the c.m. momentum of the opening channel.

The paradigm case is the simple Breit-Wigner resonance with

$$\mathcal{T}_{ij}(E) = \frac{\Gamma_i \Gamma_j / 2}{m_R - i \Gamma_{\text{tot}} / 2 - E}. \quad (1.1)$$

For narrow resonances remote from relevant thresholds the various partial widths  $\Gamma_i$  can be well approximated by constants; in general, unitarity requires energy-dependent partial widths—for  $S$ -wave channels typically of the form  $\Gamma_i = k_i \gamma_i$ , with  $k_i$  the corresponding channel c.m. momentum and the reduced width  $\gamma_i$  roughly constant. Since  $k_i$  and  $-k_i$  correspond to the same energy, yet give different values for the continued scattering amplitude, Eq. (1.1), we need to distinguish these. It is this specification of the signs of the momenta that defines the sheet structure of the energy plane. In the present discussion we are mainly concerned with two channels,  $\pi\pi$  and  $K\bar{K}$ , and we label their corresponding c.m. channel momenta by  $k_1$  and  $k_2$ . The relevant sheets are then defined by the signs of  $(\text{Im}k_1, \text{Im}k_2)$ , so that, by convention, sheet I has signs  $(+, +)$ , sheet II has  $(-, +)$ , sheet III  $(-, -)$ , and sheet IV  $(+, -)$ . For resonances remote from thresholds, there is a unique adjacent unphysical sheet and the position of the nearby resonance pole is unambiguous. In contrast for the  $f_0(S^*)$  and related cases, where the resonance adjoins the threshold of a strongly coupled inelastic channel, several unphysical sheets lie close to the resonance position and one has to specify on which sheet a given resonance pole lies.

Such poles and the sheets on which they lie form a key interface between theory and experiment. They are close to data since they emerge relatively directly by extrapolation from experimental measurements. They are objective in the sense of occurring universally at the same position in all processes to which a given resonance couples. Pending a realistic scheme for deriving bound-state properties from the fundamental Lagrangian, they provide an ideal characterization of resonance types. The Jost function [16]  $\Phi(k_2)$ , to be introduced in Sec. II, yields a very convenient parametrization, since it allows alternative resonance topologies to be enforced.

In Refs. [11,12] we proposed a way of discriminating alternative mechanisms for generating resonances, such as the  $f_0(S^*)$ , that occur just below the threshold of a strongly coupled  $S$ -wave channel. Our test is based on the number of nearby poles of the associated scattering amplitude in the complex energy plane. The rule is as follows: Molecular resonances that arise from forces between the external scattering particles (here  $\pi\pi$  and  $K\bar{K}$ ) correspond to a single nearby pole. Here, nearness is defined by the range of the forces as follows from a suitable effective range expansion [12]. As emphasized in Refs. [11,12], this rule is *not* a mathematical theorem and could doubtless be evaded by suitably complicated potentials but is likely to be satisfied for realistic physical regimes. The outcome for the present discussion is that if

the  $f_0(S^*)$  corresponds to more than one nearby pole, it is most unlikely to be a molecule.

This general approach to distinguishing alternative resonance mechanisms has a long history as detailed in Refs. [11,12]. In particular, there have been related discussions of the  $\Lambda(1405)$  baryon system [17,18]. Among previous discussions of the  $f_0(S^*)$  [19], only a few have stressed alternative pole topologies [20]; mostly this has been pre-judged by the parametrization used. A key element in our criterion for distinguishing molecular resonances is reference to the range of the relevant forces. This aspect is not considered in some previous discussions which claim to discriminate types of resonance [21].

To describe the  $S^*$  phenomenon, a nearby sheet II pole is well-nigh compulsory to reproduce the rapid movement of the  $I=J=0$   $\pi\pi$  phase shift below  $K\bar{K}$  threshold, as discussed in Sec. II. Such a pole has been a feature of all analytic descriptions of the  $S^*$  phenomenon since its key experimental manifestations were first clearly delineated [7]. There could in addition be a sheet III pole. Such a companion pole will always occur if the  $S^*$  admits a Breit-Wigner description, Eq. (1.1), but it need not lie close to the physical region and the  $K\bar{K}$  threshold at  $E=2m_K$ . Where it does lie close, its parameters form an essential part of the characterization of the resonance. This situation with nearby poles on sheets II and III runs directly counter to the  $K\bar{K}$  molecule hypothesis.

More complicated configurations with three or more poles are possible; indeed, such a solution with three poles characterized by the description of the  $S^*$  phenomenon favored by the AMP analysis [8]. This is a different kind of alternative from the one-pole-two-pole dichotomy referred to above, where one is speaking of a single resonance in either case. Adding an additional sheet II pole implies a distinct increase in complexity. No matter what indirect evidence is claimed by the excellence of a fit (and the AMP analysis spoke very strongly in this regard), direct evidence for the proposed extra narrow  $K\bar{K}$  bound state is needed before it can count as an established effect. As we shall explain, the data available have altered so as to allow a new scrutiny of all of the above questions.

This new information is of two kinds: first, as advertised by AMP [8], data on the decays  $J/\psi \rightarrow \phi\pi^+\pi^-$ ,  $\phi K^+K^-$  [22,23] could prove a powerful constraint on the underlying hadron amplitudes. At that time, only data from Mark II [24] were available with rather limited statistics. Now we have measurements from both DM2 [22] and Mark III [23] in 10-MeV bins and these will indeed provide crucial new restrictions on the  $\pi\pi \rightarrow \pi\pi$  and  $\pi\pi \rightarrow K\bar{K}$  amplitudes. Added to this we have data on  $D_s \rightarrow \pi(\pi\pi)$  decay from E691 at Fermilab [25]. In general, the addition of new precise information would be expected to constrict the range of possible amplitudes found previously by the AMP analysis still further. However, there is also new information that opens up possibility space. The  $\pi\pi \rightarrow K\bar{K}$  measurements by Etkin *et al.* [26] of the  $S$ -wave cross section were normalized by these authors in accord with the results of Cohen *et al.* [27]. Indeed, earlier experiments reporting normalized  $\pi\pi \rightarrow K\bar{K}$  measurements [28,29] broadly uphold the nor-

malization of Cohen *et al.* [27]. However, a new analysis [30] by the BNL-CCNY group of their data, supplemented by new results [31], has shown that this need not be the case and so the absolute normalization of the  $\pi\pi \rightarrow K\bar{K}$  cross section, so important in the AMP analysis, may be uncertain by up to a factor of 2.

Moreover, the reason the AMP analysis so uncompromisingly required three states in the 1-GeV region was its ability to fit the data from the AFS Collaboration [32] that tracked through the  $K\bar{K}$  threshold region more precisely than any other. This requires a simultaneous fit to the very sharp fall near 1 GeV found in central dipion production in high-energy  $pp$  collisions (Fig. 1), while also fitting the relative normalization of  $K^+K^-$  production they found. A narrow bound state in the neighborhood of  $K\bar{K}$  threshold, which is the key novel feature of the AMP solution, inevitably has a marked influence on all  $K\bar{K}$  processes very close to threshold. The first 50 MeV  $K\bar{K}$  data bin of AFS started at 1 GeV, as it was claimed the detector had negligible acceptance down toward the  $K^+K^-$  threshold. Consequently, the most marked part of the enhancement produced by a narrow state near threshold would not have been seen, though, of course, the tail above 1 GeV is. Subsequent analysis has revealed that the quoted cross section *may* in fact be that right from  $K^+K^-$  threshold to 1050 MeV [33]. Since a bound state such as that in the AMP solution would give 70% of its contribution to such a bin below 1 GeV, it is clearly important to be certain of the acceptance efficiency in this region. AFS are not alone in receiving this call for certitude in such acceptance. Many, if not all, experiments correct for efficiency by assuming a phase-space distribution. This clearly neglects the possibility of sharp dynamical features close to the  $K\bar{K}$  threshold which there undoubtedly are: a glance at the  $I=J=0$   $\pi\pi \rightarrow \pi\pi$  cross section (Fig. 1) shows that; it is just that in the AMP solution these are doubly sharp.

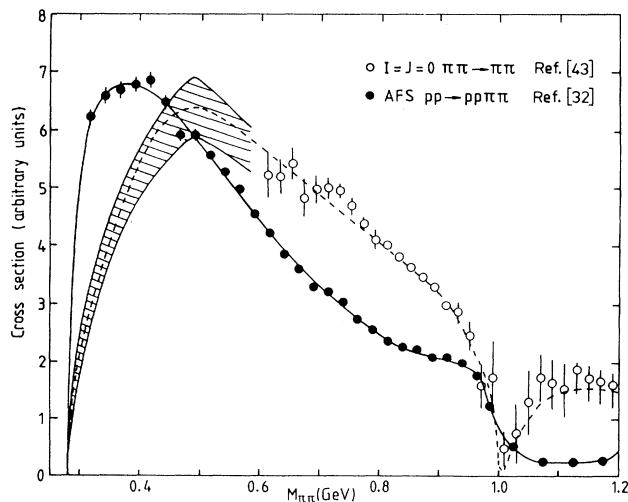


FIG. 1. Alternative indications of the  $I=J=0$   $\pi\pi$  spectrum: (a) elastic cross section inferred from peripheral dipion production [43] (○); (b) low- $t$  central production [32] (●).

With these relaxations of some of the key inputs to the AMP analysis and with the addition of precision  $J/\psi$ -decay data of the last 5 years it is timely, as recently emphasized by Burnett and Sharpe [1], to pursue a new analysis of these  $I=J=0$  channels so intimately linked by unitarity. It is this use of the all-embracing constraint of unitarity that sets both the present analysis and that of the AMP analysis apart from so many others. In particular, that by Lindenbaum and Longacre [30] neglects this constraint, assuming that this can be imposed as a  $K$  matrix afterthought. Although fine in weakly coupling perturbation theory, this is difficult to justify for such maximally strong interactions. In the fitting by the CERN WA76 Collaboration [34] (to be discussed later), data on each channel are fitted in terms of resonances and backgrounds. While the resonances are taken to transmit from one channel to another, here the backgrounds are all independent. Of course, unitarity knows of no artificial distinction between resonances and backgrounds, but relates only the total amplitudes. Such fits, lacking the tight straight jacket imposed by unitarity, not surprisingly find it is relatively easy to describe data on different channels since these are treated as having quite independent background components. Unitarity is here an all-important consideration. A key feature of our analysis (and that of AMP) is the universality of its treatment of all  $\pi\pi$  and  $K\bar{K}$  final states with the same quantum numbers however they are produced.

In Sec. II we introduce a unitary representation for the  $S$  matrix in terms of the Jost function [16]. It is the zeros of this function which describe resonance poles that transmit from one process to another. In Sec. III we assemble the data on  $I=J=0$   $\pi\pi$  and  $K\bar{K}$  channels that we fit in Sec. IV. Section V discusses our results and compares them with other analyses. Section VI reviews what these imply for the status of the scalar mesons. In Sec. VII we conclude.

## II. METHOD

### A. General formalism

To very good approximation, the only channels open to  $I=J=0$  mesons close to 1 GeV are the two-body channels  $\pi\pi$  and  $K\bar{K}$ . Other sources of inelasticity are negligible [7] until  $\eta\eta$  threshold at 1.1 GeV. To study these dynamics we shall invoke data not only on the basic hadronic scattering processes  $\pi\pi(K\bar{K}) \rightarrow \pi\pi(K\bar{K})$  but on other production reactions leading to these final states. For reasons explained later we restrict our attention to the mass range 0.87 to 1.1 GeV. As a shorthand, we henceforth refer to  $I=J=0$  as being  $f_0$  quantum numbers. The guiding principle that collates all this information is unitarity with some assistance from analyticity.

With  $\pi\pi$  and  $K\bar{K}$  the only strong interaction initial and final states we need consider below 1100 MeV, we denote these channels by 1 and 2, so that the associated  $T$ -matrix elements are

$$\begin{aligned}
\mathcal{T}(\pi\pi \rightarrow \pi\pi) &\equiv \mathcal{T}_{11}, \\
\mathcal{T}(\pi\pi \rightarrow K\bar{K}) &\equiv \mathcal{T}_{12}, \\
\mathcal{T}(K\bar{K} \rightarrow K\bar{K}) &\equiv \mathcal{T}_{22}.
\end{aligned}
\tag{2.1}$$

Although we shall be concerned with the 8-MeV energy difference between  $K^+K^-$  and  $K^0\bar{K}^0$  thresholds, the strong interaction amplitudes for these two channels are assumed equal in accord with isospin invariance [35] and so it is only their phase space that differs between them. For these basic scattering processes, unitarity requires

$$\begin{aligned}
\text{Im}\mathcal{T}_{11} &= \rho_1 |\mathcal{T}_{11}|^2 + \rho_2 |\mathcal{T}_{12}|^2, \\
\text{Im}\mathcal{T}_{12} &= \rho_1 \mathcal{T}_{11}^* \mathcal{T}_{12} + \rho_2 \mathcal{T}_{12}^* \mathcal{T}_{22}, \text{ etc.},
\end{aligned}
\tag{2.2}$$

with  $E$ , the c.m. energy, and  $\Theta$  the usual step function,

$$\rho_1 = \left[ 1 - \frac{4m_\pi^2}{E^2} \right]^{1/2} \Theta(E^2 - 4m_\pi^2)
\tag{2.3}$$

and

$$\begin{aligned}
\rho_2 &= \frac{1}{2} \left[ 1 - \frac{4m_{K^+}^2}{E^2} \right]^{1/2} \Theta(E^2 - 4m_{K^+}^2) \\
&\quad + \frac{1}{2} \left[ 1 - \frac{4m_{K^0}^2}{E^2} \right]^{1/2} \Theta(E^2 - 4m_{K^0}^2),
\end{aligned}
\tag{2.4}$$

where the superscripts  $+$  and  $0$  denote the charged and neutral kaon masses. Below  $K\bar{K}$  threshold, when  $\rho_2 \equiv 0$ , these require that the phases of the amplitudes  $\mathcal{T}_{11}$  and  $\mathcal{T}_{12}$  must be equal, which in turn implies that, for  $4m_\pi^2 \leq E^2 \leq 4m_K^2$ ,

$$\mathcal{T}_{12}(E) = \alpha(E) \mathcal{T}_{11}(E),
\tag{2.5}$$

where  $\alpha(E)$  is a real function of energy in this region. For later use, let us introduce here in addition to the  $\mathcal{T}$ -matrix elements the corresponding  $\mathcal{S}$  matrix given by

$$\mathcal{S}_{ij} = \delta_{ij} + 2i\sqrt{\rho_i\rho_j} \mathcal{T}_{ij}.
\tag{2.6}$$

For each set of production processes,  $p$ , such as  $AB \rightarrow \pi\pi$ ,  $AB \rightarrow K\bar{K}$ , we denote their amplitudes by  $\mathcal{F}_1^{(p)}$ ,  $\mathcal{F}_2^{(p)}$ , where  $p = AB$ . For such processes, unitarity imposes the linear constraint

$$\begin{aligned}
\text{Im}\mathcal{F}_1^{(p)} &= \rho_1 \mathcal{F}_1^{(p)*} \mathcal{T}_{11} + \rho_2 \mathcal{F}_2^{(p)*} \mathcal{T}_{21}, \\
\text{Im}\mathcal{F}_2^{(p)} &= \rho_1 \mathcal{F}_1^{(p)*} \mathcal{T}_{12} + \rho_2 \mathcal{F}_2^{(p)*} \mathcal{T}_{22}.
\end{aligned}
\tag{2.7}$$

Strictly, this form of unitarity only applies to nonhadronically initiated reactions, such as  $\gamma\gamma \rightarrow \pi\pi(K\bar{K})$ . However, it naturally extends to multihadron decays such as  $J/\psi \rightarrow \phi\pi\pi(K\bar{K})$ , where only two of the final-state particles undergo strong interactions, and the third, here the  $\phi$ , is merely a spectator. These notions can be further extended to central production processes, such as  $pp \rightarrow pp\pi\pi(K\bar{K})$ , which may be interpreted as a double Pomeron reaction  $PP \rightarrow \pi\pi(K\bar{K})$  (cf. Ref. [8]).

The unitarity equations, Eqs. (2.7), are satisfied by

$$\begin{aligned}
\mathcal{F}_1^{(p)} &= \alpha_1^{(p)}(E) \mathcal{T}_{11} + \alpha_2^{(p)}(E) \mathcal{T}_{21}, \\
\mathcal{F}_2^{(p)} &= \alpha_1^{(p)}(E) \mathcal{T}_{12} + \alpha_2^{(p)}(E) \mathcal{T}_{22},
\end{aligned}
\tag{2.8}$$

as a consequence of Eqs. (2.2) (Ref. [8]). Such a solution has previously been written down by Aitchison [36]. The  $\alpha_i^{(p)}(E)$  are real functions of energy for  $E^2 \geq 4m_\pi^2$ . Unitarity requires the production amplitude to have the same right-hand cut structure as the corresponding hadronic amplitude, but they will, of course, have different left-hand cuts. Consequently, the functions  $\alpha_i^{(p)}(E)$ , which we can regard as describing the coupling of the initial state  $p$  to channel  $i$ , are real along the right-hand cut. Because the functions  $\alpha_i^{(p)}(E)$  have only left-hand cuts, they can have little local variation along the right-hand cut. They can remove zeros of  $\mathcal{T}_{ij}$  that do not appear in the  $\mathcal{F}_i^{(p)}$  and similarly eliminate zeros of  $\det \mathcal{T}_{ij}$  and introduce other zeros, but only for good dynamical reasons, for instance, to satisfy the Adler condition [37]; otherwise they must be smoothly varying functions. Over the limited energy region we study here, the residual part of  $\alpha_i^{(p)}(E)$  will be represented by low-order polynomials in  $E^2$ .

To explain this simply, let us consider first the single-channel case that applies for  $4m_\pi^2 < E^2 < 4m_K^2$ , when unitarity requires

$$\mathcal{F}_1^{(p)} = \alpha_1^{(p)}(E) \mathcal{T}_{11}(E) = \alpha_2^{(p)}(E) \mathcal{T}_{12}(E)
\tag{2.9}$$

[cf. Eq. (2.5)], where the  $\alpha_i(E)$  are real for  $E^2 \geq 4m_\pi^2$ , and having only left-hand cuts must be smooth in this region. Now the amplitudes  $\mathcal{T}_{11}(E)$  and  $\mathcal{T}_{12}(E)$  have zeros close to threshold at  $E = E_{11}$  and  $E = E_{12}$ , respectively. Both are the on-shell manifestations of Adler zeros. If the smooth functions  $\alpha_i(E)$  were simply polynomials, Eq. (2.9) would imply that every production amplitude, regardless of the process, would have a zero at  $E = E_{11}$ , not to mention requiring  $E_{11} = E_{12}$ , which is, of course, not true. Thus, the  $\alpha_i(E)$  cannot be represented just by polynomials in  $E^2$ , but must contain poles to remove zeros of  $\mathcal{T}_{11}$  and  $\mathcal{T}_{12}$ . Thus we would parametrize the  $\alpha_i$ 's in this example by

$$\alpha_i(E) = \bar{\alpha}_i(E) + \frac{\lambda_i}{s - s_0},
\tag{2.10}$$

where the residual part  $\bar{\alpha}_i(E)$  can now be represented by a polynomial in  $s = E^2$  and where  $s_0 = E_{ij}^2$  and  $\mathcal{T}_{ij}(E_{ij}) = 0$ . In practice, the Adler zero [37] is the only known example of such a zero.

In the two-channel case that applies in our study we do not just have to be concerned about zeros of  $\mathcal{T}_{11}$  and  $\mathcal{T}_{12}$ , which need not transmit to the production amplitudes, but we also have to worry about the vanishing of  $\det \mathcal{T}$ . Imagine this occurs at  $E = E_0$ , where  $s_0 = E_0^2$ . Now if the  $\alpha_i$  have no pole at  $s = s_0$ , then not only would  $\mathcal{T}_{11}/\mathcal{T}_{12} = \mathcal{T}_{12}/\mathcal{T}_{22} \equiv \kappa$  at  $s = s_0$  but Eq. (2.8) would mean that  $\kappa = \mathcal{F}_1^{(p)}/\mathcal{F}_2^{(p)}$  without having to measure the couplings to these production processes—again this cannot be true. Thus, we must allow the  $\alpha_i$  to have poles, but only at the position of the vanishing of the determinant of  $\mathcal{T}$ . This can only happen below  $K\bar{K}$  threshold, where the two-channel amplitudes have related phases. In practice

we find the relevant hadronic amplitudes do have such a zero. We therefore parametrize the  $\alpha_i$ 's in a way analogous to Eq. (2.10), viz.,

$$\begin{aligned}\alpha_1^{(p)}(E) &= \bar{\alpha}_1^{(p)}(E) + \frac{\lambda^{(p)}}{s-s_0} \mathcal{T}_{12}(E_0), \\ \alpha_2^{(p)}(E) &= \bar{\alpha}_2^{(p)}(E) - \frac{\lambda^{(p)}}{s-s_0} \mathcal{T}_{11}(E_0).\end{aligned}\quad (2.11)$$

The residual parts  $\bar{\alpha}_i^{(p)}$  will be represented by low-order polynomials in  $s$ :

$$\bar{\alpha}_i^{(p)}(E) = \sum_{m=0}^{m_{\max}} \beta_{im}^{(p)} s^m. \quad (2.12)$$

Formally, all this can be expressed in terms of an eigenvalue problem [38].

A further consequence of unitarity, vital for our discussion, is that it requires that resonance poles be universal, i.e., a given resonance pole occurs at the same complex energy  $E_R$  in all processes to which it couples. This is automatically built into our solution, Eqs. (2.8). The unitarity equation, Eq. (2.2), expresses the singularity structure of  $\mathcal{T}_{ij}(E)$  that arises from successive opening thresholds. As described in the Introduction, the resulting *sheet structure* of  $\mathcal{T}_{ij}(E)$  has to be taken into account when a resonance occurs close to a threshold. For two-body scattering, the phase-space factors  $\rho_i(E)$  of Eqs. (2.2)–(2.4) contain terms  $\sqrt{E^2 - E_{\text{threshold}}^2}$  with a plus and/or minus ambiguity which feeds through into the scattering amplitudes. The statement that  $\mathcal{T}_{ij}(E)$  has a resonance pole at some complex energy  $E_R$  is therefore incomplete without specifying on which sheet it lies, as emphasized in the Introduction. In practice, the distinction only matters for a resonance close to a threshold to which it strongly couples. In other circumstances, only the pole on the adjacent unphysical sheet is important [15].

The question of the number of poles and sheet location is crucial for distinguishing resonance mechanisms in our approach [11,12]. We therefore need a parametrization for  $\mathcal{T}_{ij}(E)$  (or equivalently  $\mathcal{S}_{ij}$ ) that keeps track of these features. This is provided by the Jost function representation [16]. In this approach, one considers the scattering amplitudes as functions of  $k_1$  and  $k_2$ , the appropriate channel c.m. momenta, i.e.,

$$k_1 = \frac{1}{2} \sqrt{E^2 - 4m_\pi^2}, \quad k_2 = \frac{1}{2} \sqrt{E^2 - 4m_K^2}, \quad (2.13)$$

where  $m_\pi, m_K$  are the respective masses averaged over the charge states. Unitarity then specifies very simple forms for the corresponding  $\mathcal{S}$ -matrix elements:

$$\begin{aligned}\mathcal{S}_{11} &= J(-k_1, k_2) / J(k_1, k_2), \\ \mathcal{S}_{22} &= J(k_1, -k_2) / J(k_1, k_2), \\ \det \mathcal{S} &= J(-k_1, -k_2) / J(k_1, k_2).\end{aligned}\quad (2.14)$$

In the  $K\bar{K}$  threshold region that is the focus of the present work, there is no sign ambiguity for  $k_1$ . Consequently, the expressions  $J$  of Eq. (2.14) may be treated

merely as functions of  $k_2$ . Although  $k_2$  is defined for the average  $m_K$ , Eqs. (2.13), we make allowance for the  $K^\pm, K^0$  mass difference using the standard prescription [35]. In computing  $K\bar{K}$  cross sections and spectra we use the appropriate physical mass in the phase-space factor, cf. Eq. (2.4). With the identifications

$$\begin{aligned}J(k_1, k_2) &\rightarrow \Phi(k_2), \\ J(-k_1, k_2) &\rightarrow \Phi^*(-k_2^*), \\ J(k_1, -k_2) &\rightarrow \Phi(-k_2), \\ J(-k_1, -k_2) &\rightarrow \Phi^*(k_2^*),\end{aligned}$$

Eqs. (2.14) become

$$\begin{aligned}\mathcal{S}_{11} (\equiv \eta e^{2i\delta_{\pi\pi}}) &= \Phi^*(-k_2^*) / \Phi(k_2), \\ \mathcal{S}_{22} (\equiv \eta e^{2i\delta_{KK}}) &= \Phi(-k_2) / \Phi(k_2), \\ \det \mathcal{S} (\equiv e^{2i(\delta_{\pi\pi} + \delta_{KK})}) &= \Phi^*(k_2^*) / \Phi(k_2),\end{aligned}\quad (2.15)$$

where for later use we introduce the conventional  $\eta \exp(2i\delta)$  notation for the  $\mathcal{S}$ -matrix elements. Characterizing resonances by their value of  $k_2$ , rather than  $E$ , automatically specifies the sheet. The  $k_2$  plane, thereby, unfolds the sheet structure of the energy plane, each quadrant of the  $k_2$  plane corresponding to a distinct sheet, I–IV, of the energy plane as numbered in Sec. I (cf. also Fig. 2).

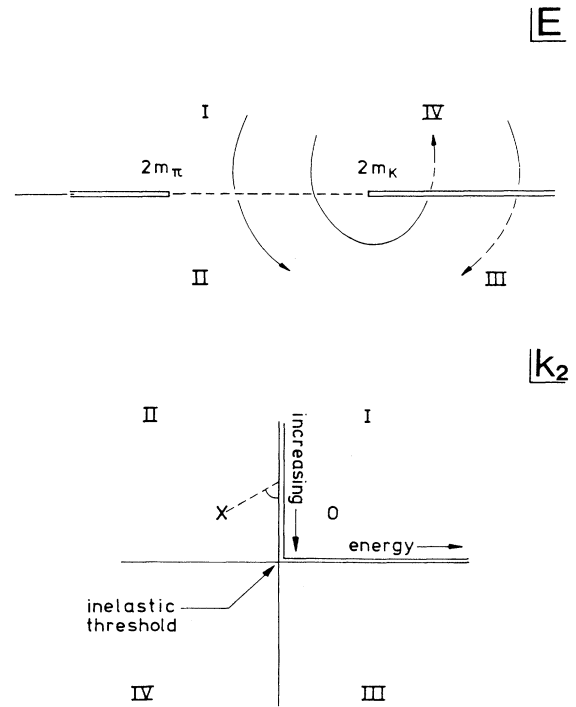


FIG. 2. Sheets of the energy ( $E$ ) plane and how they unfold into different quadrants of the  $k_2$  plane. This latter figure illustrates how a resonance pole ( $\times$ ) induces a zero of  $\mathcal{S}_{11}(0)$  at the mirror position in the imaginary axis so that the depicted angle relates to the phase shift  $\delta_{\pi\pi}$ .

Equations (2.15) immediately suggest strategies for constructing  $\Phi$ 's that manifest specific resonance characteristics. To secure a resonance pole at  $E = E_R$  on a specific sheet we only need to impose a zero of  $\Phi$  at the corresponding  $k_2$  value,  $k_2^R = \frac{1}{2}\sqrt{E_R^2 - 4m_K^2}$ . A natural way to do this is to express the Jost function as a product of terms. These terms embody both resonances and background by writing

$$\Phi = \Phi^{\text{res}}\Phi^{\text{bkgd}}, \quad (2.16)$$

where

$$\Phi^{\text{res}} = \prod_{i=1}^{n_p} \left[ 1 - \frac{k_2}{k_{2Ri}} \right] \quad (2.17)$$

appropriately having the zeros associated with poles of the  $\mathcal{S}$  matrix and representing  $\Phi^{\text{bkgd}}$  by an *entire* function, for example,

$$\Phi^{\text{bkgd}} = \exp \left[ \sum_{n=0}^{n_B} \gamma_n k_2^n \right]. \quad (2.18)$$

This ensures the  $\mathcal{S}$  matrix has no other poles than those explicitly implanted through the zeros of  $\Phi^{\text{res}}$ . The coefficients,  $\gamma_n$  of Eq. (2.18), are in general complex numbers. Inspection of Eqs. (2.15)–(2.18) reveals that the real parts of  $\gamma_n$  for even  $n$  cancel between the numerator and denominator in the  $\mathcal{S}$ -matrix elements, Eqs. (2.15). Thus, these may be set to zero. Such a representation as Eqs. (2.16)–(2.18) has a limited range of applicability. It only includes the singularities near to  $K\bar{K}$  threshold. It does not encompass  $\eta\eta$  threshold, or the more distant  $f_0(\epsilon)$  pole [39], except as a background feature. Thus for the present purpose we restrict its use (and the data we consider) to the range  $0.87 \leq E \leq 1.1$  GeV. The product form of  $\Phi$ , Eq. (2.16), means we can attribute specific contributions to the inelasticity  $\eta$  and to the phase shifts  $\delta_{\pi\pi}$  and  $\delta_{KK}$  arising from each pole and from the background. That the ensuing  $\eta$  and  $\delta_{\pi\pi}$  ( $\delta_{KK}$ ) be in accord with physical requirements places restrictions on the parameters entering  $\Phi$ . Obvious stipulations are that there are no poles on the physical sheet and that  $|\eta| \leq 1$ . This latter condition has to be probed each time parameter values are changed. This is an undoubted practical disadvantage of the Jost function representation but, for the present purpose, more than compensated by having the number and type of poles under control.

A further requirement is that the background's energy variation should be physically reasonable, such as could arise from available exchanges and from broad resonances that couple to our system. We shall take *background* phase variation of (say)  $30^\circ$  over and within the range from  $K\bar{K}$  threshold to 1.1 GeV as the maximum possible for both  $\delta_{\pi\pi}$  and  $\delta_{KK}$ .

### B. Signatures and characterizations of inelastic $S$ -wave resonances

Before proceeding to the details of our analysis and the description of the results, we briefly review some general aspects of resonance characterization. In this we have

two main objectives: to recall key features of other work and the philosophies that inform them and to provide an intuitive feel for how our analysis actually distinguishes alternative resonance types. Most of the following discussion applies to all situations where an  $S$ -wave resonance adjoins a strongly coupled inelastic threshold, not only  $f_0(S^*)$  but its companion  $0^{++}$  meson,  $a_0(\delta)$ , and  $\frac{1}{2}^-$  baryons such as  $\Lambda$  (1405),  $N$  (1535), and  $\Sigma$  (1750). Some of the aspects to be commented upon show more clearly for these other cases, notably  $a_0(\delta)$ . In particular,  $f_0(S^*)$  shows in its elastic channel  $\pi\pi \rightarrow \pi\pi$  as a dip rather than a bump owing to the substantial background phase,  $\delta_B \approx 90^\circ$ , that is present. In order to see  $f_0(S^*) \rightarrow \pi\pi$  as a peak one needs to view a suitable production or decay reaction, e.g.,  $J/\psi \rightarrow \phi\pi\pi$  (see Fig. 8).

The first aspect that we discuss is the quantitative characterization of resonances—the mass, width, branching ratios, and so forth—that one may and should assign to the observed experimental signals. According to viewpoint, widely different values are extracted from the same experimental information; thus for the  $a_0(\delta)$ , width values ranging from 50 to several hundred MeV are inferred on the basis of the same data. Let us recall how these divergences arise.

The most efficient primary characterization of a resonance  $R$  is in terms of its complex resonance poles

$$E_R = M_R - i\Gamma_R/2. \quad (2.19)$$

These quantities are known to be highly stable against changes in the parametrization of the physical cross sections [40]. They are therefore the optimal quantities for comparing signals of a given resonance  $R$  from different processes and experiments; wherever possible they should have pride of place in compilations such as the Particle Data Group tables. If more than one pole controls the resonance, all need to be supplied and the sheet specified. In what follows we will indicate this by an appropriate suffix:  $E_R^N \equiv M_R^N - i\Gamma_R^N/2$  ( $N = \text{II, III}$ ). There is in principle additional information in the complex residues,  $c_{1,2}$  of the scattering amplitude at each pole  $E_R^N$ , but because of the way unitarity constrains the amplitudes, it is only of secondary interest; we therefore do not emphasize the residues in what follows but concentrate on the resonance poles.

The relation between such poles and characteristic resonant features of the data is very direct in the Jost representation of the  $\mathcal{S}$ -matrix elements, Eq. (2.15). Suppose, for example, that  $\Phi(k_2)$  is controlled by poles on sheets II and III and a background phase (thus a sort of cut-down version of our actual two-pole fit to be described below). The diagonal  $\mathcal{S}$ -matrix elements are then given by

$$\begin{aligned} \mathcal{S}_{11} &= \prod_{N=\text{II, III}} \left[ \frac{1 + k_2/k_{2R}^N}{1 - k_2/k_{2R}^N} \right] \exp(2i\delta_B), \\ \mathcal{S}_{22} &= \prod_{N=\text{II, III}} \left[ \frac{1 + k_2/k_{2R}^N}{1 - k_2/k_{2R}^N} \right]. \end{aligned} \quad (2.20)$$

Each pole supplies a multiplicative factor to  $\mathcal{S}_{11}$  and  $\mathcal{S}_{22}$  and these have an obvious geometrical interpretation in

terms of the  $k_2$ -plane mapping of the energy plane (lower part of Fig. 2). In particular, for  $\mathcal{S}_{11}$ , the pole at  $k_{2R}^N$  is necessarily accompanied by a zero at  $-k_{2N}^{R*}$ . Thus the phase shift  $\delta_{\pi\pi}(E)$  is directly related to the angle subtended by the line joining  $k_2(E)$  to  $k_{2R}$  (Fig. 2). This is why a sheet II pole is needed to describe the rapid phase movement associated with the  $f_0(S^*)$  below  $K\bar{K}$  threshold and why the associated pole parameters are the best determined characteristics of  $f_0(S^*)$ . The existence and location of any additional sheet III pole is a much more delicate issue only to be decided by detailed confrontation with data such as we describe below (cf. Sec. IV).

The notation  $M_R, \Gamma_R$  of Eq. (2.19) is intended to evoke the concepts of mass and width but other measures of these quantities play an obvious role. For resonances of the type considered here these can differ appreciably. In the first place, there are the observed peak position  $M_{\text{obs}}$  and corresponding full width at half maximum into the elastic channel,  $\Gamma_{\text{obs}}$ . These have the obvious merit of relating directly to experiment but vary from process to process. Alternative, more theoretically tinged parameters  $m_0, \Gamma_0$ , and  $g_2^2/g_1^2$  arise when a Breit-Wigner (BW) description with energy-dependent widths is employed. Although this has been a popular parametrization since the pioneering discussion of  $a_0(\delta)$  by Flatté [41], it would not serve for our present main purpose, since it is rather restrictive and, in particular, its use prejudices the number of poles (the two-channel BW form necessarily has poles on sheets II and III). However, it does highlight conventional resonance parameters and also furnishes a very convenient two-pole example to contrast with a one-pole description. Let us consider these two aspects in turn.

The (BW) description entails a Jost denominator

$$\Phi(s) = [m_0^2 - s - i\rho_1 g_1^2 - i\rho_2 g_2^2] e^{-i\delta_B}. \quad (2.21)$$

Aside from the background phase, this bears the canonical three parameter for a simple inelastic resonance—the mass  $m_0$  and the two coupling constants  $g_1, g_2$ . In place of  $g_1$ , the corresponding *true partial width*  $\Gamma_0$  to the lighter channel

$$\Gamma_0 = g_1^2 \rho_1(m_0) / m_0 \quad (2.22)$$

is often cited. How does such a three-parameter description relate to the four parameters from the resonance poles  $E_R^{\text{II}}$  and  $E_R^{\text{III}}$  of Eq. (2.19)? (By sending  $E_R^{\text{III}}$  to infinity we include the one-pole case in the following discussion.)

We can provide a schematic answer to this question by matching the expressions for the simplified Jost function of Eq. (2.20) and the (BW) version of Eq. (2.21). For this idealized case we find that  $k_{2R}^{\text{II}}$  and  $k_{2R}^{\text{III}}$  depend on just three parameters:

$$k_{2R}^{\text{II}} = -\alpha + i\beta, \quad k_{2R}^{\text{III}} = \alpha - i\gamma. \quad (2.23)$$

If we further assume all  $k_2$  momenta are small we discover

$$g_1^2 = 4\alpha(\gamma + \beta), \quad g_2^2 = 4m_K(\gamma - \beta), \quad (2.24)$$

and (inserting  $\rho_1 \approx 1$ )

$$\Gamma_0 = (\Gamma_R^{\text{II}} + \Gamma_R^{\text{III}}) / 2. \quad (2.25)$$

Provided  $g_2^2$  is not too large ( $g_2^2 \ll 4m_K[m_K^*(m_R^{\text{II}} - m_R^{\text{III}})]^{1/2}$ ), we also obtain

$$m_0 = (m_R^{\text{II}} + m_R^{\text{III}}) / 2. \quad (2.26)$$

Finally, from Eq. (2.24),

$$\frac{g_2^2}{g_1^2} = \left[ \frac{m_K}{\alpha} \right] \left[ \frac{\gamma - \beta}{\gamma + \beta} \right]. \quad (2.27)$$

We propose Eqs. (2.25)–(2.27) as working definitions even when using more complicated and realistic Jost formulas such as the data require. Although the above detailed identifications do not then all apply [since the real parts of  $k_{2R}^{\text{II}}$  and  $k_{2R}^{\text{III}}$  are no longer related precisely as in Eq. (2.23), we use  $\alpha = \text{Re}(k_{2R}^{\text{III}} - k_{2R}^{\text{II}}) / 2$  when evaluating Eq. (2.27)], qualitative features should remain valid. Thus,  $k_{2B}^{\text{III}}$  should lie deeper than  $k_{2R}^{\text{II}}$  [ $\gamma > \beta$  from Eq. (2.24)] and consequently  $\Gamma_R^{\text{III}}$  be larger than  $\Gamma_R^{\text{II}}$ . This explains why  $E_R^{\text{III}}$  is harder to establish and fix than  $E_R^{\text{II}}$ : another reason for giving primacy to the separate pole parameters of  $E_R^{\text{II}}$  and  $E_R^{\text{III}}$ . In discussing the  $a_0(980)$ , Flatté [41] and other authors [42] have stressed that  $\Gamma_0$  will certainly be larger and may be much larger than the corresponding observed width which is narrowed by cusp effects from the opening  $K\bar{K}$  channel. This is reflected in Eq. (2.25) through  $\Gamma_R^{\text{III}}$  being larger than  $\Gamma_R^{\text{II}}$ .

We can study such effects in the context of the (BW) model of Eq. (2.21). A simple exercise along these lines explicitly directed to  $f_0(S^*)$  phenomenology is described below.  $E_{S^*}^{\text{II}}$  is held fixed at a typical value and  $C \equiv g_1^2/g_2^2$  varied. Some resulting  $E_{S^*}^{\text{III}}$  and  $m_0, \Gamma_0$  values are listed in Table I. In addition to the trends already mentioned,  $m_0$  is seen to come out increasingly smaller than  $m_R^{\text{II}}$  as  $C \rightarrow 0$ , a kind of mass renormalization implicit in the (BW) formalism.

Similar renormalizations occur in Törnqvist's prescription [2] for modeling how final-state interaction effects distort meson spectroscopy but work in the opposite sense so that his bare masses come out larger than the observed ones. For the scalar family, his specific objective was to demonstrate that a conventional ( $0^{++}$ ) nonet could be reconciled with unconventional appearances by

TABLE I.  $S$ -wave resonance coupling to an opening inelastic channel; influence of relative squared coupling to the elastic and inelastic channels ( $g_1^2/g_2^2$ ) on Breit-Wigner parameters ( $m_0, \Gamma_0$ ) and sheet III pole position  $E_R^{\text{III}} \equiv M_R^{\text{III}} - i\Gamma_R^{\text{III}}/2$  in a simple model [Eq. (2.21)] with *fixed sheet II pole* specified by  $M_R^{\text{II}} = 988$  MeV and  $\Gamma_R^{\text{II}} = 48$  MeV.

$C$ $\equiv g_1^2/g_2^2$	$m_0$ (MeV)	$\Gamma_0$ (MeV)	$m_R^{\text{III}}$ (MeV)	$\Gamma_R^{\text{III}}$ (MeV)
0.3	959	102	852	230
0.5	976	70	953	98
1.0	983	57	977	66
5.0	987	50	986	52

making appropriate allowance for final-state interactions. He did this by modifying (BW) propagators in a model dependent but not unreasonable way. Nowadays, there are simply too many scalars for such a picture to be the whole story but some variant may still have a role in interpreting the observed spectrum.

We now turn to the second topic of this subsection: understanding via illustrative examples how measurements of the phase,  $\delta_{\pi\pi}$ , and inelasticity,  $\eta$ , allow different pole topologies to be discriminated. We therefore compare an amplitude with one pole in the  $k_2$  plane (and no other structure) with a family of amplitudes containing two poles. For the latter we use the (BW) form equation Eq. (2.21) referred to above. The ratio ( $g_1^2/g_2^2$ ) of the squares of the couplings to channels 1 and 2 is the variable we call  $C$ . To make these models close to the real case we consider in Sec. III, the one-pole and two-pole amplitudes are constructed to have the same sheet II pole at  $E^{\text{II}}=0.988-0.024i$  GeV and the phase  $\delta_{\pi\pi}=176^\circ$  at  $K\bar{K}$  threshold. While both amplitudes have this sheet II pole, only that given by the Breit-Wigner formula has

a sheet III pole. When  $C$  is large, this pole is mirror symmetric in the  $k_2$  plane with the sheet II pole, i.e.,  $k_2^{\text{III}}=-k_2^{\text{II}}$ . However, as  $C$  decreases the sheet III pole moves further away from the origin at  $K\bar{K}$  threshold, coming within the ambit of the rule stated in Sec. I. Furthermore, in the limit  $C\rightarrow 0$ , this pole has moved off to infinity and the amplitude becomes the one-pole form. Thus, by considering a family of two-pole amplitudes with variable ratio  $C$  we can see the effect of the second pole.

Our model amplitudes for various ratios of couplings,  $C$ , give the phase shift  $\delta_{\pi\pi}$  and inelasticity  $\eta$  shown in Fig. 3. These plots highlight how the behavior of these observables is quite different, if  $C$  is small or large. Indeed, the variation is sufficiently marked that it is not unrealistic to believe that experimental data can distinguish these possibilities. In Sec. III we detail the data we use for this purpose.

### III. DATA SELECTION

The deep and narrow minimum in the  $I=J=0$   $\pi\pi$  elastic cross section (Fig. 1) coupled with the sharp onset of inelasticity at  $K\bar{K}$  threshold [7] inescapably signals a narrow dynamical structure strongly coupling to the  $K\bar{K}$  channel. This is the  $f_0(S^*)$ , the nature and parameters of which we aim to determine in this analysis. In principle, highly precise data on the three reactions:  $\pi\pi\rightarrow\pi\pi$ ,  $\pi\pi\rightarrow K\bar{K}$ , and  $K\bar{K}\rightarrow K\bar{K}$  would suffice for this task. The information on such processes is extracted from experimental results on high energy dimeson production at small momentum transfers, where these reactions are controlled by one-pion exchange or one-kaon exchange. Although high statistics experiments, notably by the CERN-Munich Collaboration [43] and by LASS [44], have been performed, the information on  $I=J=0$  channels is the least well determined in any partial wave analysis. Scrutiny of narrow effects requires good energy resolution. However, such dimeson production experiments do not provide this, 20-MeV bins being typical.

What is more, a glance at the compilation of  $\pi\pi\rightarrow K\bar{K}$  cross sections (with  $f_0$  quantum numbers) in Fig. 4 illustrates how poorly these are known. Moreover, even an experiment with enormous statistics, such as LASS [44], yields merely a handful of events on  $K^+K^-\rightarrow K_s^+K_s^-$  near threshold. Thus, the  $T$ -matrix elements are underconstrained by these classic meson-meson scattering data. Consequently, one casts the net wider to encompass production processes and decays. It is at this point that the extended unitarity of Sec. II, Eq. (2.7), is involved, since this relates all channels with  $\pi\pi$  and  $K\bar{K}$  final states. Many such production processes and decays not only favor the quantum numbers of interest, but also allow fine-energy resolution so essential for delineating narrow effects. Notable among these reactions is central dimeson production in  $pp\rightarrow pp(M_1M_2)$ . At very small momentum transfers and at high energies, this process is dominated by double Pomeron exchange ensuring the dimeson final state has  $I=0$ . Data on this process in this ultralow  $|t|$  domain are provided only by the AFS Colla-

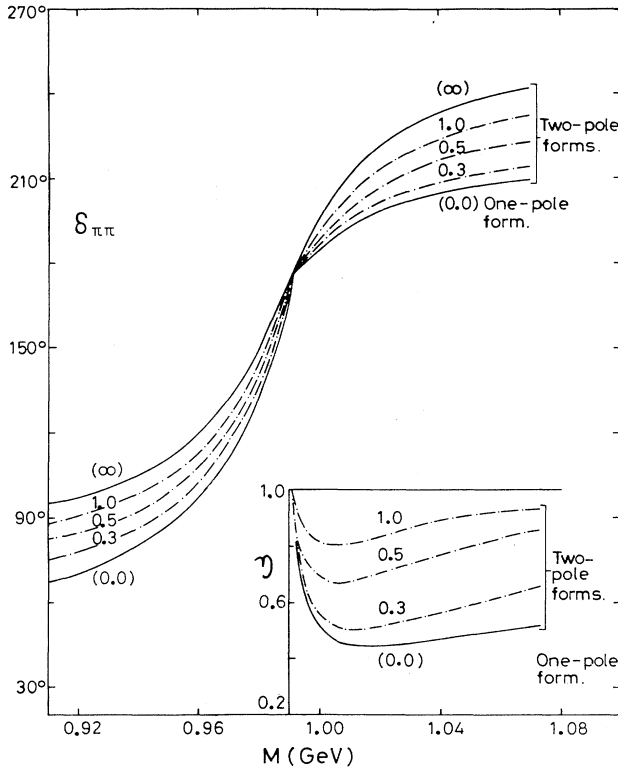


FIG. 3. Different ways a resonance can couple just below an inelastic threshold illustrated by simple models. The curves showing  $\delta_{\pi\pi}$  and  $\eta$  vs  $M(\equiv\sqrt{s})$  correspond to alternative one- and two-pole forms possessing a sheet II pole at  $988-24i$  MeV and yielding a phase shift  $\delta_{\pi\pi}=176^\circ$  at threshold. These requirements fix the chosen one-pole form, which is based on a constant  $K$  matrix, and reduces the variability of the two-pole form adopted (Breit-Wigner with a channel 1 background phase) to a single parameter,  $C\equiv g_1^2/g_2^2$  by which the two pole curves are labeled.  $C=0$  recovers the one-pole form.



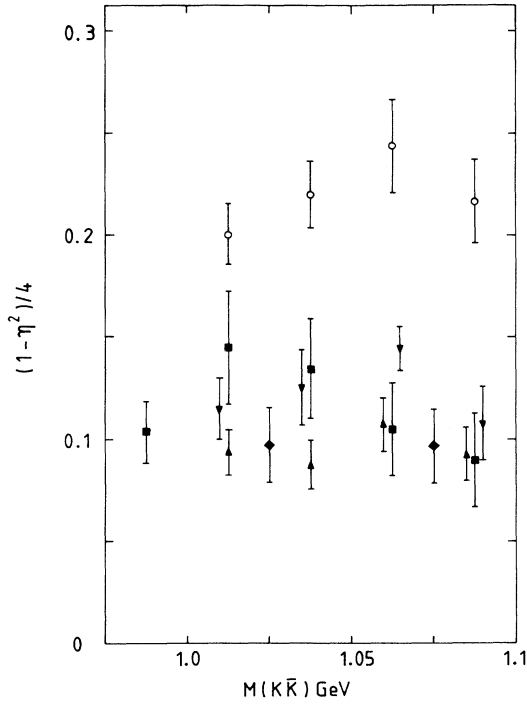


FIG. 4. Compilation of  $\pi\pi \rightarrow K\bar{K}$   $I=0$   $S$ -wave cross-section measurements expressed in terms of  $1/4(1-\eta^2)$  vs  $K\bar{K}$  mass: (■) Cohen *et al.* [27], (▼) Etkin *et al.* [26] (as normalized in [26]), (▲) Polychronakos *et al.* [29], (◆) Wetzel *et al.* [28], (○) Longacre *et al.* [30].

boration [32]. Here too the  $\pi\pi$  cross section has a precipitous fall in the 1-GeV region (Fig. 1).

Unitarity not only forces a close conformity between such production amplitudes and those of meson-meson scattering, but it does so for decay amplitudes too when all final-state particles other than  $\pi\pi$  and  $K\bar{K}$  act as spectators. Thus a most valuable addition to our analysis is the decay  $J/\psi \rightarrow \phi\pi\pi(K\bar{K})$  [22–24]. Experiments allow a 10-MeV mass resolution with reasonable statistics and the DM2 results [22] are confirmed by Mark III [23]. In terms of the quark line rule, these processes may be viewed as  $s\bar{s} \rightarrow \pi\pi(K\bar{K})$  or equivalently off-shell “ $K\bar{K}$ ”  $\rightarrow \pi\pi(K\bar{K})$ . Thus, these data are a natural supplement to the *less than perfect*  $\pi\pi \rightarrow K\bar{K}$  information. Moreover, the dynamical structure near 1 GeV appears as a sizable peak (not a dip) in the  $\pi\pi$  channel (in conformity with the quark line rule expectation). Conceptually, the decay  $D_s \rightarrow \pi(\pi\pi)$  is very similar and has been measured by Anjos *et al.* [25]. Thus we include their results too, though information on the related  $D_s \rightarrow \pi(K\bar{K})$  mode is not reported.

On the face of it, the radiative decay  $J/\psi \rightarrow \gamma\pi\pi$  would provide the ideal constraint along these lines. Unfortunately, this final state can be confused with  $\pi^0(\pi\pi)$ , in which only one photon from the  $\pi^0$  decay is detected. This contamination is dominated by the mode  $J/\psi \rightarrow \pi^0\rho^0$ , which, having a sizable branching ratio, distorts the  $\pi\pi$  mass spectrum in the region we consider

(viz.  $E \in [0.87, 1.1]$  GeV). Consequently, we have to exclude these data. Other decay modes, such as  $J/\psi \rightarrow \omega\pi\pi$ , on which copious data have been taken, have no inactive spectator in the final state. Since they have overlapping cross bands on the Dalitz plot, computing their final-state interactions is a complicated problem in three-body dynamics, which does not simply constrain the  $\mathcal{T}_{ij}$ .

We now give a catalogue of the specific data with  $f_0$  quantum numbers we use in our analysis. These are grouped in four sectors labeled henceforth by (a)–(d).

(a) Classic meson-meson scattering. This effectively supplies 105 data points, as follows.

$\pi\pi \rightarrow \pi\pi$ : The phase-shift  $\delta_{\pi\pi}$  and inelasticity  $\eta$  from (i) the energy-independent analysis of the CERN-Munich data [43] and (ii) from the experiment of Cason *et al.* [45].

$\pi\pi \rightarrow K\bar{K}$ : The cross section in the form of  $(1-\eta^2)/4$  from the experimental results of (i) Cohen *et al.* [27], (ii) Etkin *et al.* [26] (as normalized in Ref. [30]), (iii) Longacre *et al.* [30], (iv) Polychronakos *et al.* [29], (v) Wetzel *et al.* [28]. These are compared in Fig. 4 and commented on below. The partial-wave analyses of these experiments also determine the  $S$ - $D$  wave phase difference  $\phi_{SD}$  which we use too.

$K^+K^- \rightarrow K_S K_S$ : The LASS experiment provides results on  $K^-p \rightarrow K_S K_S \Lambda$ , as analyzed by Aston *et al.* [44], which we assume can be related, up to an energy independent constant, to the corresponding  $K^+K^- \rightarrow K_S K_S$   $I=0$   $S$ -wave cross section.

All told, there are 63 items of raw data in this sector, but we give  $\pi\pi$  phase and inelasticity information enhanced weight because our input for these is only a selection of what is available.

Where there are data from more than one experiment, these are in agreement, except in the case of  $\pi\pi \rightarrow K\bar{K}$ . Consequently, we need to comment on how we treat these latter data. As seen from the compilation of Fig. 4, the  $\pi\pi \rightarrow K\bar{K}$  cross-section results are in general accord apart from that of Longacre *et al.* [30] (note, however, that the earlier BNL/CCNY results of Etkin *et al.* [26] were actually normalized to those of Cohen *et al.* [27] in Ref. [26] and used by AMP, cf. Fig. 8 of Ref. [26]). Rather than distort our fits by using inconsistent data sets we have been advised [46] to apply a free normalization, to be called  $K$  in Sec. IV, to the results of Longacre *et al.* [30] and to those of Etkin *et al.* [26] as reinterpreted in [30]. We will comment on what happens if this is not done in Sec. IV B below. In addition the partial-wave analyses of these same  $K\bar{K}$  experiments determine the  $S$ - $D$  interference. In the region of interest, the  $I=0$   $D$  wave is controlled by the  $f_2(1270)$  resonance with known phase variation. We parametrize this using the form given in Ref. [8], Eq. (3.24).

(b) Central dimeson production provides nine data points as follows.

$pp \rightarrow pp\pi\pi(K\bar{K})$ : Cross-section results from the AFS collaboration on central dimeson production as analyzed by Cecil [32]. As discussed in Sec. I, the status of the first  $K^+K^-$  datum has changed. In the AMP analysis [8], it was taken to be the cross section in the energy bin from

1.0 to 1.05 GeV. It is now believed to be that from  $K^+K^-$  threshold up to 1.05 GeV [33].

(c)  $J/\psi$  decays with 81 data points as follows.

$J/\psi \rightarrow \phi\pi\pi(K\bar{K})$ : Dimeson mass distributions from DM2 [22], Mark III [23], and Mark II [24]. These results have not been partial-wave analyzed, but are assumed to have  $J=0$ .

(d)  $D_s$  decay with 9 data points as follows.

$D_s \rightarrow \pi(\pi\pi)$ :  $\pi\pi$  mass distribution from the Fermilab experiment E691 by Anjos *et al.* [25]. Again these results have not been partial wave analyzed, but are assumed to have  $I=J=0$ .

#### IV. FITS: ALTERNATIVE TYPES OF SOLUTIONS COMPARED

##### A. Choice of parametrization

Operationally, the task we have set ourselves is to devise alternative one-, two-, and three-pole fits to the above collection of  $I=J=0$   $\pi\pi$  and  $K\bar{K}$  scattering and production data covering the dimeson mass range 0.87 to 1.1 GeV. The data to be fitted will be considered in the four broad sectors (a)–(d) just listed in Sec. III. These supply a total of 204 data points.

Our detailed parametrization follows exactly the method outlined in Sec. II [Eqs. (2.15)–(2.18), (2.6), (2.8), (2.11), (2.12)]. We require one group of parameters to specify the basic  $\pi\pi(K\bar{K}) \rightarrow \pi\pi(K\bar{K})$  scattering amplitudes,  $\mathcal{T}_{ij}$ , which within our method means constructing the Jost functions, Eq. (2.15)–(2.18). A second group of parameters is then needed to relate the various production processes ( $p$ ) that we invoke [data sectors (b), (c), and (d) of Sec. III] to the  $\mathcal{T}_{ij}$ . According to Eq. (2.8) that entails providing for each production process ( $p$ ) the coefficients for the *effective coupling functions*  $\alpha^{(p)}(E)$  [the  $\beta$ 's and  $\lambda$  of Eqs. (2.11) and (2.12)], where necessary augmented by overall normalization coefficients for individual experiments. We allocate the corresponding fit parameters as follows.

Sector (b): Central dimension production ( $PP \rightarrow M_1M_2$ ) five parameters.

Sector (c):  $J/\psi \rightarrow \phi M_1M_2$  seven parameters. Sector (c) involves three experiments, each of which requires its own overall normalization to be fitted since only the event distribution is given in each case. Consequently, the treatment of the number of parameters is equivalent to that for (b).

Sector (d): For  $D_s \rightarrow (M_1M_2)\pi$  with much less data and only the  $\pi\pi$  final state we allow three parameters.

The above 15 parameters appear in all our fits. In addition we have the special renormalization parameter  $K$  used with the BNL-CCNY (1987)  $\pi\pi \rightarrow K\bar{K}$  data [30] and a normalization constant  $C_K$  referred to above, needed to relate data on  $K^-p \rightarrow K_S K_S \Lambda$  [44] to the associated  $K\bar{K} \rightarrow K\bar{K}$  cross section. This gives 17 parameters in all.

It remains to specify the Jost function,  $\Phi$  of Eqs. (2.15)–(2.18), and consequently the  $\mathcal{T}$ -matrix elements  $\mathcal{T}_{ij}$ . This is the point at which one-, two-, and three-pole alternatives we consider are implanted by allowing the corresponding number of complex zeros in  $\Phi^{\text{res}}$ , Eq.

(2.17). We then need to select a form for the associated background contribution, Eq. (2.18). In this, our concern is to compensate for the additional fit parameters that extra zeros bring. In total,  $\Phi$  receives  $n_\Phi = 2n_p + n_B$  parameters from its  $n_p$  poles and  $n_B$  background coefficients, Eqs. (2.17) and (2.18). For our one-, two-, and three-pole fits to be reported below the allocations are 1 pole (fit 1)  $n_\Phi = 11$  ( $n_p = 1, n_B = 9$ ), total number of fit parameters 28, 2 pole (fit 2)  $n_\Phi = 8$  ( $n_p = 2, n_B = 4$ ), total number of fit parameters 25, and 3 pole (fit 3)  $n_\Phi = 10$  ( $n_p = 3, n_B = 4$ ), total number of fit parameters 27. These are deployed in fitting our 204 data points. Notice that fit 1, to be reported below, has several more parameters than those of fit 2, in particular. Our first attempts at fitting used equal numbers, but fit 1 proved so inadequate that we added extra background coefficients.

##### B. Results

Extracting genuine minima of  $\chi^2$  for such a heterogeneous data collection and relatively complicated parametrization is far from straightforward and some care was needed to achieve our alternative one-, two-, and three-pole fits. Our results are as follows (see Table II and Figs. 5–8). Inspecting first the results for the total  $\chi^2$  per degree of freedom, we see that a two-pole type of fit (fit 2) is strongly preferred giving a very adequate  $\chi^2/N_{\text{DF}}$  of 1.12. The corresponding 3-pole (fit 3) and 1-pole (fit 1) fits are appreciably poorer with  $\chi^2/N_{\text{DF}}$  values, respectively, of 1.56 and 1.72. (In terms of the actual values of  $\chi^2$ , fit 1 is 5 standard deviations and fit 3 is 4 standard deviations poorer than fit 2.) The outstanding feature of fit 2 is its success with the production processes (b), (c), and (d) as borne out by the  $\chi^2/N_{\text{DF}}$  for the corresponding sectors (Table II) and the associated fits (Figs. 6–8). It could fairly be stated that these experiments, especially those yielding information on  $J/\psi \rightarrow \phi\pi\pi$  [22,23] (Fig. 8), provide the clearest signal for the  $f_0(S^*)$  of any data that are available. It is these same data that

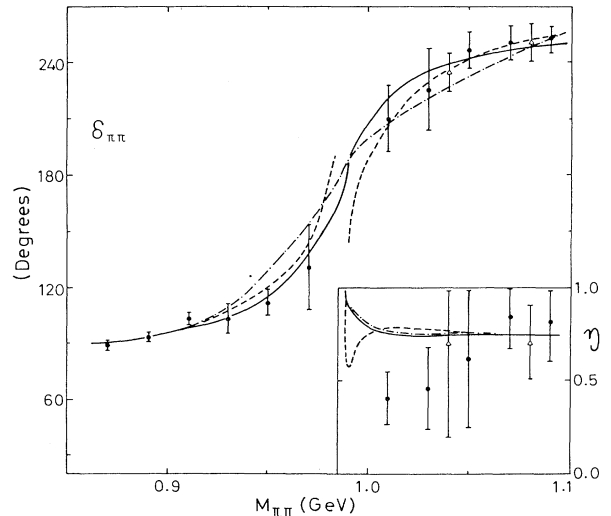


FIG. 5.  $I=J=0$   $\pi\pi$  phase shifts,  $\delta_{\pi\pi}$ , and inelasticity,  $\eta$ , according to our fits: fit 1 (---), fit 2 (—), fit 3 (---) compared to data from [43] (●) and [45] (△).

TABLE II.  $\chi^2$  breakdown for the alternative fits described in the text. Each is the optimal specimen of its type characterized by the number of resonance poles on sheet II ( $n^{\text{II}}$ ) and sheet III ( $n^{\text{III}}$ ). Columns 3–6 list  $\chi^2$  contributions from individual data sectors: (a) “elastic” information, (b) central production, (c)  $J/\psi$ , and (d)  $D_s$  decays; corresponding  $\chi^2/N_{\text{DF}}$  values are written below in square brackets.

Fit	No. of parameters	Sector contributions to $\chi^2$				$\chi^2_{\text{tot}}$	$\chi^2/N_{\text{DF}}$
		(a)	(b)	(c)	(d)		
Fit 1 (one pole) $n^{\text{II}}=1, n^{\text{III}}=0$	28	154 [1.64]	17 [4.25]	130 [1.81]	2 [0.33]	303	1.72
Fit 2 (two poles) $n^{\text{II}}=1, n^{\text{III}}=1$	25	130 [1.34]	2.2 [0.55]	66 [0.92]	3.1 [0.52]	201	1.12
Fit 3 (three poles) $n^{\text{II}}=2, n^{\text{III}}=1$	27	94 [0.99]	16 [4.0]	152 [2.11]	14 [2.33]	276	1.56
No. of data points		(105)	(9)	(81)	(9)	(204)	

play the key role in disfavoring fit 1 as compared to fit 2 with  $\chi^2/N_{\text{DF}}$  almost doubled for this sector (c). (To see how this arises requires close inspection of Fig. 8.) Fit 3 is likewise heavily disfavored by the  $J/\psi$  decay data and also somewhat by central dimeson production data and  $D_s$  decay information. Note that the central production results were the very data that, in the AMP analysis [8], indicated a three-pole solution. It is likely that this difference mainly arises from the revised information on

the  $K\bar{K}$  acceptance near threshold discussed in Sec. I.

The domain where fit 2 is less successful than fit 3 is the combined scattering data, sector (a); fit 2 scores  $\chi^2/N_{\text{DF}}=1.36$  to fit 3's 1.0 and fit 1's 1.64. As already discussed, this subset of data is the most problematic, lacking the detailed precision and compatibility to discriminate solution types and fix resonance parameters definitively. A glance at Figs. 5, 6, and 7(d) showing  $K^-p \rightarrow K_S K_S \Lambda$  spells out the problem. Even the  $\pi\pi$

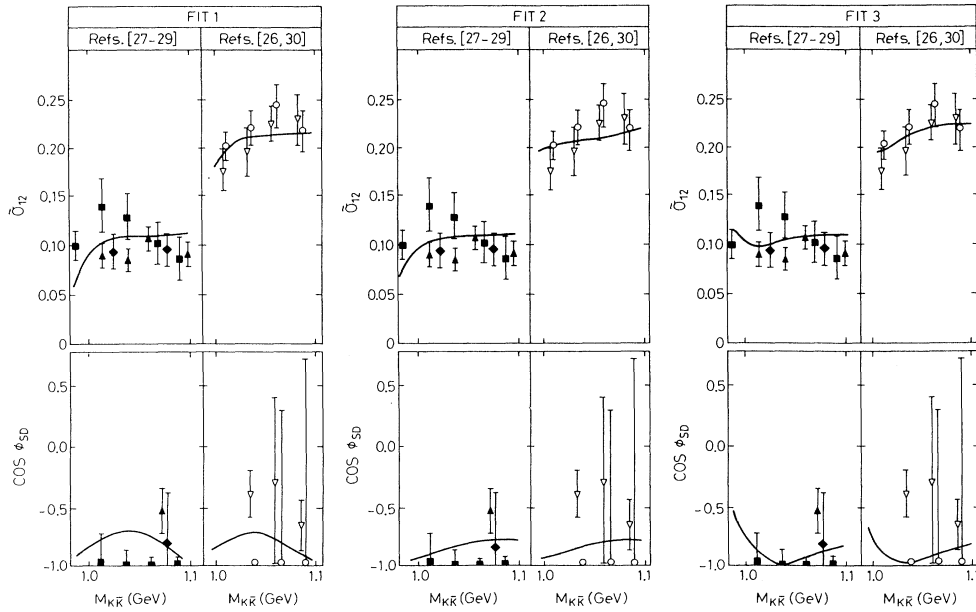


FIG. 6. Fits to  $I=J=0$   $\pi\pi \rightarrow K\bar{K}$  information from [27] ( $\blacksquare$ ), [28] ( $\blacklozenge$ ), [29] ( $\blacktriangle$ ), [26] (as normalized in [30]) ( $\nabla$ ) and [30] ( $\circ$ ). The upper plots show the values reported for  $\hat{\delta}_{12} \equiv (\frac{1}{4})(1-\eta^2)$ . (For fitting to the data from [26] and [30] a common overall rescaling factor was allowed and the measured  $\hat{\delta}_{12}$  fitted to  $(K/4)(1-\eta^2)$  with  $K$  chosen by the fit; results for  $K$  were 1.93 (fit 1), 1.91 (fit 2), 1.98 (fit 3).) The lower plots refer to  $SD$  interference expressed as  $\cos\phi_{SD} \equiv \cos(\phi_S - \phi_D)$  with  $\phi_D$  taken from a conventional Breit-Wigner form (cf. [8] Eq. (3.24)) using standard  $f_2$  (1270) parameters.

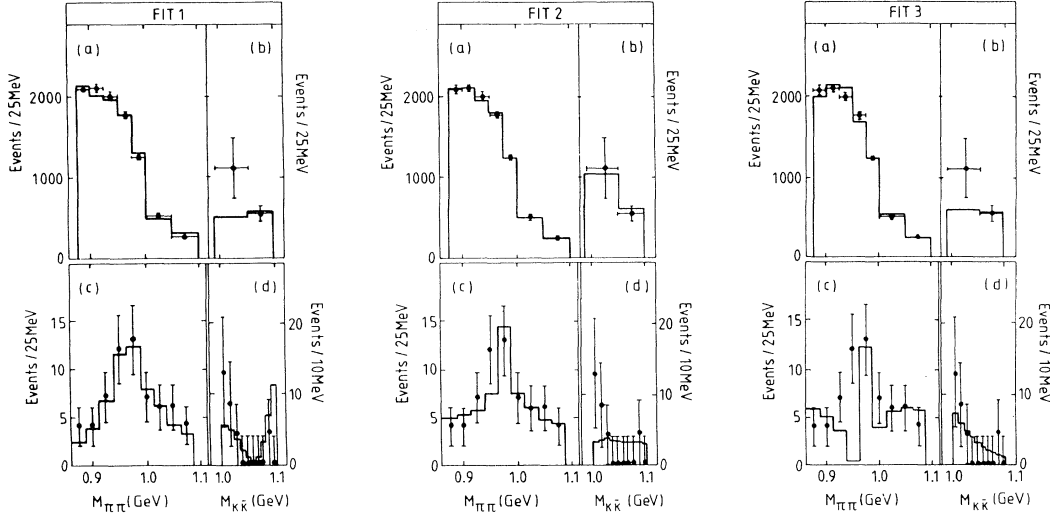


FIG. 7. Fits to various production processes compared to data: (a) and (b) central dimeson production  $pp \rightarrow pp\pi\pi$  and  $K\bar{K}$  from [32]; (c)  $\pi\pi$  spectrum from  $D_s \rightarrow \pi\pi(\pi)$  decay from [25]; and (d)  $K\bar{K}$  production in  $K^-p \rightarrow K_S^0 K_S^0 \Lambda$  from [44].

phase-shift information on  $\delta_{\pi\pi}$  and  $\eta$  is missing and imprecise just where it is needed most. Above all, various experiments bearing on the crucial  $\pi\pi \rightarrow K\bar{K}$  input have large discrepancies in overall normalization as mentioned in Secs. I and III. Fit's 1, 2, and 3 were all generated allowing a free overall normalization,  $K$ , for the BNL-CCNY information [30] on  $(1-\eta^2)/4$ . If this freedom is removed, the  $\chi^2$  increases appreciably; for the two-pole fit  $\chi^2/N_{DF}$  goes from 1.12 to 1.9 with the increase coming entirely from the  $\pi\pi \rightarrow K\bar{K}$  sector where  $\chi^2$  increases nearly threefold.

An alternative approach to the discrepant  $\pi\pi \rightarrow K\bar{K}$  information is to decide that the two groups of data segregated on Fig. 6 (respectively, Refs. [27–29] and [26,30]) cannot both be right as to their overall normalization. In our main fits we have assigned the normalization uncer-

tainty to the BNL-CCNY analysis [30]. If, instead, we take the published BNL-CCNY normalizations and allow a free (overall) normalization to the data of Refs. [27–29],  $\chi^2$  is still increased but not markedly; for a two-pole fit  $\chi^2/N_{DF}$  goes from 1.12 to 1.30. Perhaps surprisingly, the pole positions are little affected.

The result of our fitting is that fit 2 is strongly favored over fit's 3 and 1 in terms of  $\chi^2$ . However, it is the superior internal consistency of the fit 2 amplitudes that makes it so compelling, as we now discuss.

### C. Selection of preferred solution type

The AMP description of the  $f_0(S^*)$  (with two resonances, three poles) [8] is not favored by the present enlarged and modified data set. As a distinctly nonminimal

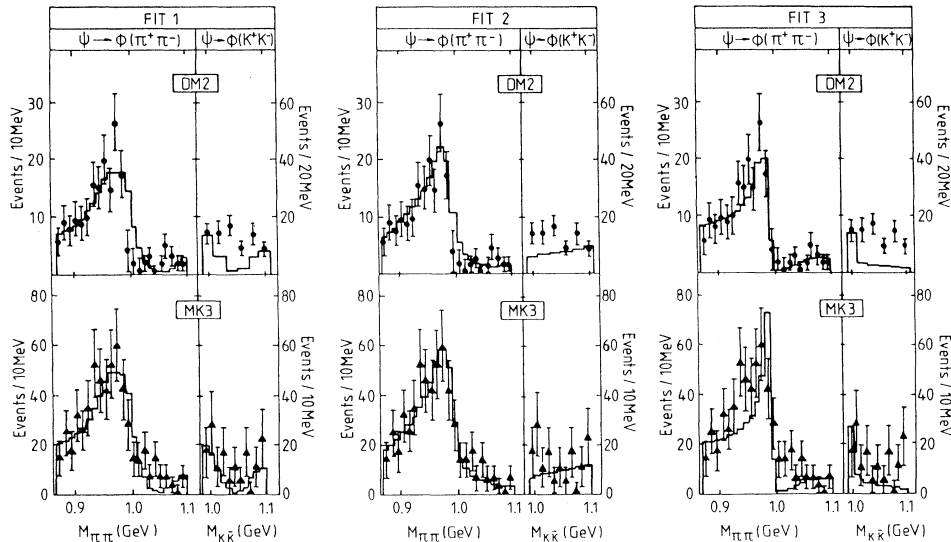


FIG. 8. Fits to data on  $J/\psi \rightarrow \phi\pi\pi(K\bar{K})$  production [assuming the final  $\pi\pi(K\bar{K})$  system is all  $I=0$   $S$  wave]: (●) data from [22], (▲) data from [23].

description of the  $S^*$  region, it must now be reckoned an unlikely runner. This finding could be upset if the hint of a sharp peak at threshold in  $K^-p \rightarrow K_S^- K_S \Lambda$  [Fig. 7(d)] were to be confirmed in this or any other reaction with  $K\bar{K}$  final states (e.g., Fig. 8).

We now seek to distinguish alternative descriptions of the  $f_0(S^*)$  using the test involving the existence and location of additional sheet III poles outlined in Sec. I. As will be recalled we aim to distinguish the two possibilities that the  $f_0(S^*)$  is (a) a  $K\bar{K}$  molecule and (b) a primary QCD compound. As will further be recalled, the essence of our test is as follows: a molecular description should have only one nearby pole (which necessarily lies on sheet II). A system that possesses nearby poles on sheets II and III cannot be a molecule; therefore, it must be a primary QCD compound, such as a  $q\bar{q}$ ,  $qq\bar{q}\bar{q}$ , or pure glue state. We have already reported first results from such a test [11] concluding that the molecule description of the  $f_0(S^*)$  is disfavored. Subsequent fitting, reported here, has merely served to reinforce our earlier conclusion. Our two-pole fit has actually improved from that reported in Ref. [11], fit 2 now has  $\chi^2/N_{\text{DF}}=1.12$  (Ref. [11]

had 1.32); fit 1 remains unchanged at  $\chi^2/N_{\text{DF}}=1.72$ . The margin of preference for fit 2 has markedly improved.

We note that fit 2 does not merely possess two poles, but two *nearby* poles in the sense of our rule. Both pole positions for fit 2 have  $|k_2| \leq 0.13$  GeV (Fig. 11); for comparison, the range  $R$  used in the Weinstein-Isgur  $K\bar{K}$  potential calculations [4] is 0.8 fm yielding  $(\hbar c)R^{-1}=0.25$  GeV.

The final step in selecting a two-pole description comes from detailed examination of the various components of the phases and inelasticity depicted in Fig. 9. This exhibits for fit's 1, 2, and 3, the components of  $\delta_{\pi\pi}$ ,  $\delta_{KK}$ , and  $\eta$  arising from poles and background. [Recall that a given pole (or background) contributes additively to the  $\delta$ 's and multiplicatively to  $\eta$ , cf. Eq. (2.15).] For the present purpose we concentrate on the plots for fit's 1 and 2, noting that for fit 2 the background is smooth and small, as befits a background. The background for fit 1 is, in contrast, highly structured and large (see especially  $\delta_{KK}$ ) with a behavior strongly akin to that arising from the sheet III pole in fit 2. Background phase variations of fit 1 over the energy range considered far exceed the  $30^\circ$  limit that we estimated as reasonable on the basis of known broad resonances and thresholds (cf. Sec. II). We thus conclude that fit 1 looks unphysical. Attempts to make the background amplitude in fit 1 less structured dramatically decreases the quality of the fit. Thus its comparative success in fitting such a wide range of data is only achieved by the background amplitudes mimicking what the sheet III pole of fit 2 naturally provides. This not only rules out the molecular ascription for the  $f_0(S^*)$  of fit 1 but highlights the internal consistency of fit 2. Thus  $\chi^2$  is not alone in pointing to a two pole, Breit-Wigner-like, resonance, but the whole structure of the amplitudes speaks to this. It is this that compels the preference for a nonmolecular assignment for the  $f_0(S^*)$ .

## V. COMMENTARY ON THE RESULTS

### A. Pole structures in fit's 1, 2, and 3

All the poles featured in our fit's 1, 2, and 3 are listed in Table III in the form  $E_R^N \equiv M_R^N - i\Gamma_R^N/2$ . Also shown is the pole position extracted by the present authors from scattering amplitudes supplied by Weinstein and Isgur [47] using their  $K\bar{K}$  picture of the  $f_0(S^*)$  [4]. As would be expected, there is just one pole near threshold, which lies on sheet II.

All the above pole locations, together with the Particle Data Group (PDG) 1992 average discussed below [48], are shown on the energy plane in Fig. 10, along with the corresponding information from the three-pole solution of AMP [8]. Sheet II poles are depicted by solid symbols, sheet III poles by open symbols with alternative fits distinguished according to the legend given in the figure caption. Figure 11 shows the same poles (omitting those from the AMP analysis) in terms of the channel 2 c.m. momentum,  $k_2$ , extended to complex values. This conveniently distinguishes the sheets of the complex  $E$  plane and affords a clear visual presentation of the sheet

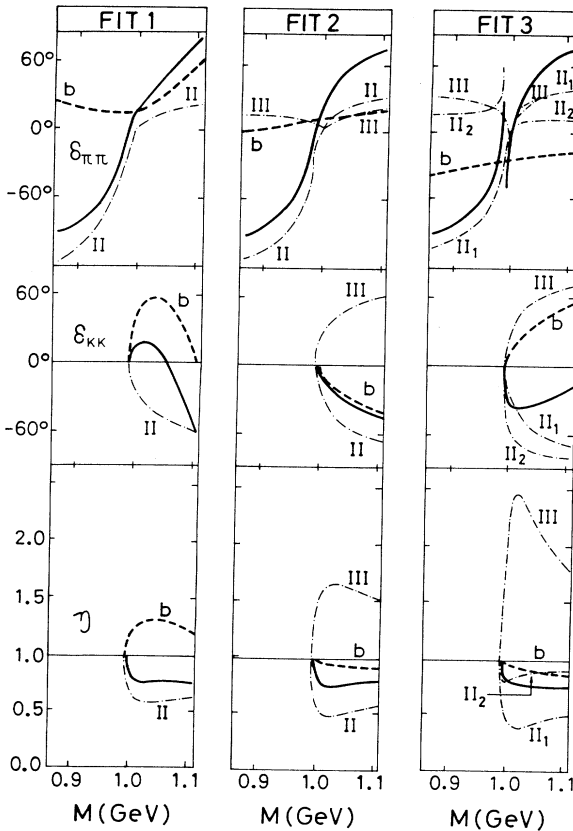


FIG. 9. Pole and background components of the fitted  $\pi\pi \rightarrow \pi\pi$  phase shift,  $\delta_{\pi\pi}$ ,  $K\bar{K} \rightarrow K\bar{K}$  phase shift,  $\delta_{KK}$ , and inelasticity,  $\eta$ , as functions of  $M \equiv \sqrt{s}$  for fit's 1, 2, and 3 discussed in the text. The various additive components of  $\delta_{\pi\pi}$  and  $\delta_{KK}$  are labeled II (III) from the poles on the corresponding sheets (dash-dot lines),  $b$  from the background (dashed) with the resulting total represented by the full line. Likewise for the multiplicative factors of  $\eta$ . For fit 3 the two sheet II pole contributions are distinguished as  $\text{II}_1$  and  $\text{II}_2$ .

TABLE III.  $f_0(S^*)$  resonance pole determinations expressed in terms of c.m. energy,  $E$ , and  $K\bar{K}$  momentum,  $k_2$ . [Note that the above PDG value is not a strict average of  $E_{S^*}^{\text{II}}$  values (see text).]

Source	$E_{S^*}^N \equiv M_{S^*}^N - i\Gamma_{S^*}^N/2$ (MeV)	$(k_2)_{S^*}^N$ (MeV)
Fit 1	$E_{S^*}^{\text{II}} = 970 - i42$	$-78 + i130$
Fit 2	$E_{S^*}^{\text{II}} = 988 - i24$ ( $\pm 10$ ) ( $\pm 6$ )	$-71 + i83$
	$E_{S^*}^{\text{III}} = 978 - i28$	$65 - i105$
Fit 3	$E_{S^*}^{\text{II}} = 994 - i29$	$-88 + i82$
	$E_{S^*}^{\text{III}} = 993 - i24$	$79 - i75$
	$E_{S^*}^{\text{IV}} = 988 - i2$	$-12 + i42$
WI model [4,47] see text	$E_{S^*}^{\text{II}} = 972 - i16$	$-37 + i105$
PDG'92 average [48]	$E_{S^*}^{\text{av}} = 974 - i24$ ( $\pm 3$ ) ( $\pm 5$ )	$-53 + i107$

II/sheet III dichotomy. To assist in relating the  $k_2$ -plane presentation to  $E$ -plane quantities, contours of constant  $\text{Re}E$  and  $\text{Im}E$  are superposed on Fig. 11.

Inspection of these results prompts the following comments.

(i) Despite the considerable additions to the input data employed (notably in the department of  $J/\psi \rightarrow \phi\pi\pi(K\bar{K})$

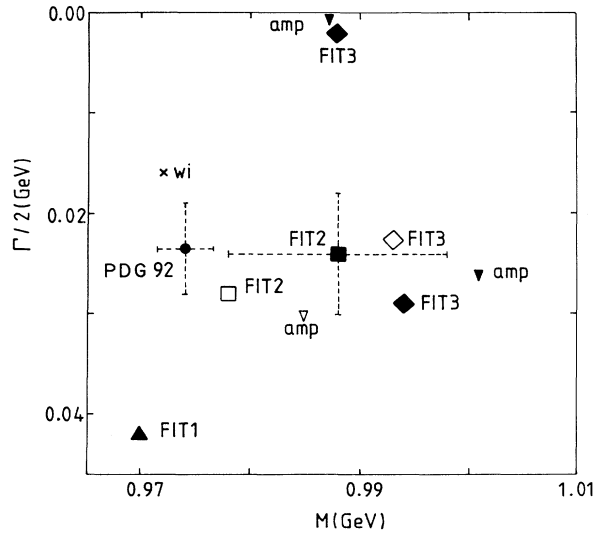


FIG. 10. Alternative  $f_0(S^*)$  resonance pole determinations compared. In each case, the pole  $E_{S^*}^N \equiv M_{S^*}^N - i\Gamma_{S^*}^N/2$  is displayed on the complex energy plane with sheets II and III superimposed. Solid symbols denote sheet II poles, open symbols sheet III poles. The legend is, for the present fits, ( $\blacktriangle$ ) (fit 1), ( $\blacksquare$ ) ( $\square$ ) (fit 2), and ( $\blacklozenge$ ) ( $\diamond$ ) (fit 3); these are compared to the previous three-pole fit ( $\blacktriangledown$   $\blacktriangledown$   $\blacktriangledown$ ) from the AMP analysis, the PDG'92 average [48] ( $\bullet$ ), and the one-pole description from the Weinstein-Isgur (WI) model ( $\times$ ) [4,47].

decays [22,23]), our present three-pole solution differs only slightly from AMP. In settling for this compromise, a very poor fit to the new data is achieved. As compared to AMP, the most significant change is an increased width for the still very narrow bound state at 0.988 GeV.

(ii) In general, findings for the principal  $f_0(S^*)$  sheet II pole are very similar for two- and three-pole solutions.

(iii) One of the most extreme solutions shown in Fig. 10 is our own one-pole fit (fit 1) with its large width and low mass. Like the three-pole solution (fit 3), this describes the  $J/\psi$  data rather poorly, emphasizing the nontrivial extent to which these data reinforce fit 2. A version of Weinstein and Isgur's potential model reported by Weinstein [49] is presumably representative in also giving a very poor description of the  $J/\psi$  results.

The sheet III poles arising in the present solutions, fit's 2 and 3, lie at approximately mirror locations to their sheet II counterparts, Fig. 11. This is, of course, a special feature of the present fits. Most published fits of the  $f_0(S^*)$  use Breit-Wigner parametrizations, commonly of the Flatté form [41], which necessarily have a sheet III pole somewhere, but not usually close to  $K\bar{K}$  threshold.

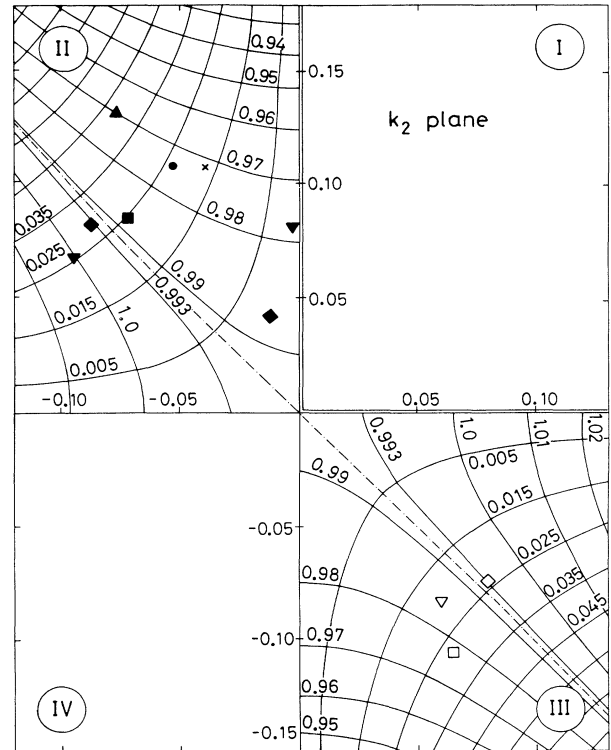


FIG. 11.  $f_0(S^*)$  resonance pole positions shown on the  $k_2$  plane ( $k_2$  denotes the  $K\bar{K}$  c.m. momentum). Points are labeled as on Fig. 10. The various sectors of the  $k_2$  plane are labeled by the corresponding sheets of the energy plane  $E \equiv M - i\Gamma/2 \equiv 2[k_2^2 + m_K^2]^{1/2}$  which are distinguished by the associated signs of  $\text{Im}k_1$  and  $\text{Im}k_2$ : ( $++$ ) (sheet I), ( $-+$ ) (sheet II), ( $--$ ) (sheet III), and ( $+ -$ ) (sheet IV). The families of faint curves superimposed on sheets II and III correspond, respectively, to constant  $M$  and  $\Gamma/2$  and are labeled in GeV accordingly.

As already emphasized, it is the fact that our sheet II and III poles are both nearby that renders our rule applicable and allows the inference that the  $f_0(S^*)$  is not a molecule. This configuration of poles in the simple form of fit 2 seems to be demanded by the new sectors of data ( $J/\psi \rightarrow \phi\pi\pi(K\bar{K})$  [22,23] and  $D_s \rightarrow 3\pi$  [25]) now available.

### B. Where experiment needs reinforcing

Before regarding the matter as settled, it is worth emphasizing that there are still gaps and discrepancies in our knowledge particularly as concerns  $K\bar{K}$  final states. First, information on the process  $\pi\pi \rightarrow K\bar{K}$  is still inadequate and contradictory (cf. Fig. 4). Furthermore, one should note that the present fits undershoot all  $K\bar{K}$  signals near threshold (Figs. 6–8). What is needed to improve this situation is enhanced statistics on  $K\bar{K}$  channels. The fact that the  $f_0(S^*)$  occurs close to 1 GeV means that a markedly different behavior is predicted for the  $K^+K^-$  and  $K_S K_S$  signals and experiments that probe these close to threshold would be invaluable.

WA76 provides just such experimental information on central dimeson production in  $\pi^-p$  and  $pp$  collisions at the CERN Super Proton Synchrotron (SPS) [34]. Using the  $\Omega'$  spectrometer, they have far better angular acceptance and better particle identification than, for instance, the CERN Intersecting Storage Rings (ISR) AFS experiment [32]. Thus their data on  $\pi^+\pi^-$ ,  $K^+K^-$ , and  $K_S K_S$  production are potentially a most valuable addition to such studies. The fits of the WA76 group to their own data already feature in the PDG average for the  $S^*$  parameters discussed below. However, as described in the Introduction, their fits supply a free background to each partial wave unconstrained by unitarity. As a consequence, they ascribe a rather tiny fraction of their  $K\bar{K}$  signal to the  $f_0(S^*)$  (see Fig. 8(b) of Ref. [34]), when this signal *must surely* be dominated by  $f_0$  quantum numbers (see our Figs. 5–8).

To include their data in our unitary analysis would require the  $\pi\pi$  final state to have  $I=J=0$ . It was already known (and is now confirmed by WA76) that such quantum numbers are most readily produced at the smallest momentum transfers. Inclusion of the WA76 data thus requires (a) the extrapolation of their results from  $-0.09 > t > -1$  GeV<sup>2</sup> to the very small  $|t|$  bite of AFS [32], i.e.,  $|t| \leq 0.015$  GeV<sup>2</sup>; a daunting task as each  $M^2$  bin appears to have a distinct  $t$  dependence or (b) the  $J=0$  quantum numbers should be first projected out of the angular distribution in each  $t$  bin. We would naturally expect the smallest  $|t|$  to have the largest and hence most significant  $S$ -wave signal. The data on both  $\pi\pi$  and  $K\bar{K}$  could then be included in our treatment, with the coupling functions  $\alpha_1, \alpha_2$  expected to have a simple exponential  $t$  dependence, but where the slope of this may vary with  $M^2$ —though in some smooth way. Thus the  $I=J=0$  data on  $d^2\sigma/dt dM^2$  could be fitted by  $\alpha_1(M^2, t)$ ,  $\alpha_2(M^2, t)$ , in which at  $|t| \leq 0.015$  GeV<sup>2</sup> these had the  $M^2$  dependence required by the AFS data.

Since projecting out the  $J=0$  final state (or at least the elimination of the odd angular momentum components)

appears to be more tractable, option (b) above should be more favorable. This in turn would allow a complete analysis of the WA76 data [34] in most of its  $|t|$  range.

### C. $f_0(S^*)$ resonance parameters compared to previous findings

Since present data indicate that the  $f_0(S^*)$  resonance is of the two-pole type, we need to specify both pole positions to characterize it. Our favored solution, fit 2, yields the following<sup>1</sup> values for the  $E^N \equiv M^N - i\Gamma^N/2$ :

$$\begin{aligned} E_{S^*}^{\text{II}} &= 988(\pm 10) - i24(\pm 6) \text{ MeV} , \\ E_{S^*}^{\text{III}} &= 978 - i28 \text{ MeV} . \end{aligned} \quad (5.1)$$

We now examine how our results compare with previous findings listed in the current (1992) Particle Data Group tables [48]. This compilation blurs the distinction between the sheet II pole parameters ( $m_{S^*}^{\text{II}}, \Gamma_{S^*}^{\text{II}}$ ) and the effective Breit-Wigner quantities ( $m_0, \Gamma_0$ ) of Eqs. (2.25) and (2.26). Both types of parametrization feature among the individual contributions to the mass and width averages that it recommends:  $m_{S^*} = 974.1 \pm 2.5$  MeV,  $\Gamma_{S^*} = 47 \pm 9$  MeV (PDG'92 average—subject to the above qualifications). However, one of PDG's sources (Armstrong *et al.* [34]) give both numbers from their analysis—for the mass  $m_0 = 979 \pm 4$  MeV and  $m_{S^*}^{\text{II}} = 1001 \pm 2$  MeV. This 22-MeV difference is possibly typical thus undermining the PDG average at this level of precision. We urge PDG to remedy this confusion in future compilations.

In Fig. 12 we ignore the above distinction and plot all the listed quantities as if they referred to the components of  $E_{S^*}^{\text{II}}$ . [We do however plot from the analysis of Armstrong *et al.* [34] their respective findings for ( $m_0, \Gamma_0/2$ ) and ( $m_{S^*}^{\text{II}}, \Gamma_{S^*}^{\text{II}}/2$ ) to illustrate the above-mentioned distinction.] Quite apart from this methodological detail, we would question the philosophy that has governed PDG's selection of inputs to their average. The classic results from amplitude analyses of high statistics peripheral dipion production experiments [50,51] are excluded; instead, the published average is dominated by signals extracted from various inclusive experiments. In several of these, the claimed  $f_0(S^*)$  signal is a minor superposition on a large background, yet quite high precision is claimed for the ensuing resonance parameters. Whether the background is small or large, standard methods for removing it must surely introduce bias to small widths.

Having said all this, the resulting comparison depicted in Fig. 12 [52] (to which we have added the omitted peripheral dipion contributions [50,51]) is quite encouraging—as regards the sheet II pole determination.

However, as we have stressed, it is the existence and lo-

<sup>1</sup>Only for the  $E_{S^*}^{\text{II}}$  parameters whose values from other analyses are extensively tabulated did we carry out the lengthy exercise of determining error ellipses.

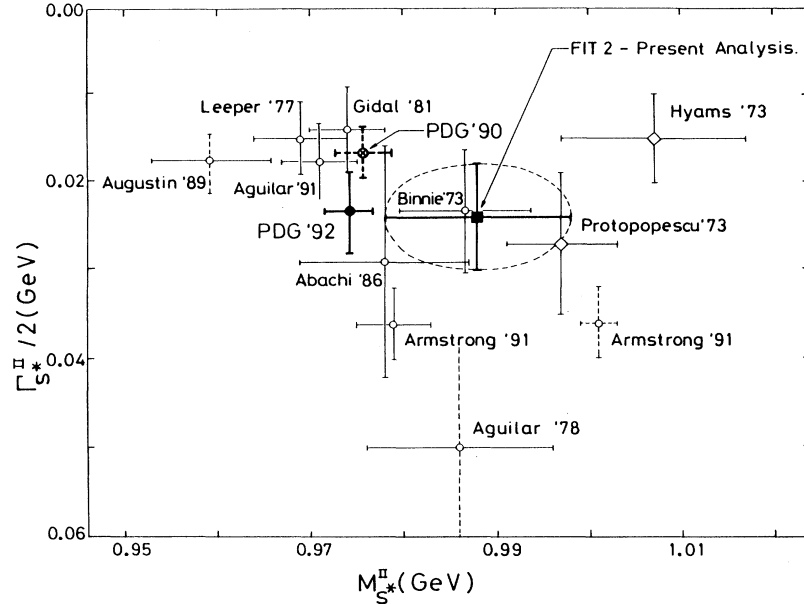


FIG. 12. Various reported measurements of  $f_0(S^*)$ 's sheet II pole position  $M_{S^*}^{\Pi} - i\Gamma_{S^*}^{\Pi}/2$  (GeV) compared: (■) value (with errors) from the present favored solution (fit 2); (●) the latest (1992) PDG average [48] (cf. remarks in Sec. V C); (⊗) the previous PDG average [52], (○) various experiments featuring in the PDG average [48], (◇) notable experiments that do not enter the PDG average [50,51] (see text for further discussion and explanations).

cation of the corresponding sheet III pole that really discriminates alternative resonance types. On that, there is no systematic compilation from other analyses with which we can compare. Where such information has been supplied, the sheet III pole occurred much deeper than for the present analysis. The present preference for approximately mirror pole locations is driven by the new data that we have included.

Given the presently favored values Eq. (5.1) we can evaluate the corresponding effective Breit-Wigner parameters from the prescription given in Eqs. (2.25)–(2.27). In this way we find

$$\begin{aligned} m_0(S^*) &= 983 \text{ MeV} , \\ \Gamma_0(S^*) &= 52 \text{ MeV} , \\ (g_2^2/g_1^2)_{S^*} &\simeq 0.85 . \end{aligned} \quad (5.2)$$

These are the values that we will use when attempting to place the  $f_0(S^*)$  spectroscopically, the topic to which we now turn.

## VI. CONSEQUENCES FOR SCALAR SPECTROSCOPY

How does the  $f_0(S^*)$  emerging from the above analysis fit into our present knowledge of the scalar family? In the following section we first make a rapid survey of the scalars, then examine possible spectroscopic assignments for the  $f_0(S^*)$ , and how alternatives might be distinguished.

### A. Light scalar mesons (1992)—a rapid survey

Table IV lists the contemporary menu of light scalars ( $0^{++}$ ) according to PDG'92 [48]. The same information

together with certain comments and comparisons with the analogous tensor states ( $2^{++}$ ) are exhibited in Fig. 13. The range of influence of each resonance is designated by the energy segment ( $m - \Gamma/2$ ,  $m + \Gamma/2$ ) to indicate potential overlap. New features for 1992 are the increased confidence in  $f_0$  (1590) [53] and the transfer of the level at 1710 MeV (formerly the  $\theta$ ) from the tensor to the scalar family [54], transmuted into  $f_0$  (1710). Our remarks on scalar classification will not consider these two states, although they will need to feature in any final description.

The scalar family has long presented a problem for

TABLE IV. Scalar mesons below 2 GeV according to PDG'92 [48]. ● denotes states considered confirmed.

State	$m$ (MeV)	$\Gamma$ (MeV)	Modes/BR's
$I=0$			
● $f_0$ (975)	974	$47 \pm 9$	$\pi\pi$ 78%, $K\bar{K}$ 22%
$f_0$ (1240)	1240	140	$K\bar{K}$
● $f_0$ (1400)	1400	150–400	$\pi\pi$ 93%, $K\bar{K}$ 7%, $\eta\eta$ seen
$f_0$ (1525)	$\sim 1525$	$\sim 90$	$K\bar{K}$
● $f_0$ (1590)	$1587 \pm 11$	$175 \pm 19$	$\eta\eta$ , $4\pi^0$ , $? \eta\eta'$
● $f_0$ (1710)	$1709 \pm 5$	$146 \pm 5$	$K\bar{K}$ , $\pi\pi$ , $\rho\rho$ seen
(Was $\theta$ )			
$I=\frac{1}{2}$			
● $K_0^*$ (1430)	$1429 \pm 6$	$287 \pm 23$	$K\pi$ 93%
$K_0$ (1950)	$1945 \pm 20$	$201 \pm 34 \pm 79$	$K\pi$ (52±14)%
$I=1$			
● $a_0$ (980)	$983 \pm 2$	$57 \pm 11$	$\eta\pi$ , $K\bar{K}$ seen
$a_0$ (1320)	$\sim 1320$	$\sim 130$	$\eta\pi$ , $?K\bar{K}$



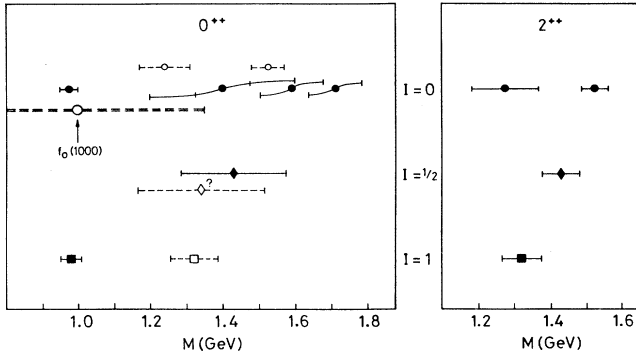


FIG. 13. Scalar and tensor mesons below 2 GeV according to PDG'92 [48]. “Confirmed” states are shown as solid symbols, unconfirmed states are depicted by open symbols. Each resonance is depicted by the segment  $(m - \Gamma/2, m + \Gamma/2)$  to indicate its range of influence and show where reported signals overlap. Also shown are the  $f_0(1000)$  ( $\epsilon$ ) resonance for the inclusion of which we have argued and the alternative characterization of  $K_0^*(1430)$  reported by [58].

spectroscopic classification owing to its unusual features. The new synthesis that emerged a few years ago [10] disposed of these problems in an attractively simple fashion by a radical reassignment of the available levels. The first step was to banish  $f_0(S^*)$  and  $a_0(\delta)$  from the world of  $(q\bar{q})$  excitations by picturing them as  $(K\bar{K})$  molecules [4]. (The authors of this model stress that it emerged naturally and unexpectedly from their nonrelativistic quark model calculation of  $K\bar{K}$  scattering.) This molecular picture neatly explains the very similar masses, close proximity to  $K\bar{K}$  threshold and isolation from other levels (see Fig. 13) of these two states. (This latter point, the isolation of the  $f_0(S^*)$ , we shall challenge below.) However, there are other schemes [55] which make the  $a_0$  and  $f_0$  special with almost degenerate masses requiring no appeal to the long-range forces so necessary for molecules.

The second step was to find substitute candidates for the vacated slots in the ground state  $(q\bar{q})$  scalar nonet. To this end, two fairly recently discovered scalar candidates  $a_0(1320)$  [56] and  $f_0(1525)$  [57] were pressed into service. Neither signal rates PDG's *confirmed* ( $\bullet$ ) status, since each has been seen in just one experiment and has doubt-raising characteristics (same mass and width as co-present and dominant tensor). If confirmed, they will be the lynch pins of the new scheme and experiments to resolve their status deserve a high priority. Given these two additions to the family of  $(q\bar{q})$  scalars and with the resonance parameter values ascribed to the remaining ground-state candidates  $f_0(1400)$  and  $K_0^*(1430)$ , one has all the ingredients to assemble a totally standard scalar nonet closely akin to its tensor counterpart. Seemingly the  $(q\bar{q})$  scalars are *normal* after all and exhibit standard quark model mass and mixing patterns.

To maintain such a view, one has to decide how to assign all the other  $f_0$  levels of Fig. 13 and to what extent the various signals reported really correspond to distinct dynamical entities. As Fig. 13 is intended to emphasize,

there is considerable overlap between the  $f_0$  claimants above 1.2 GeV (confirmed and unconfirmed). Clearly one has to await a comprehensive unitary analysis of all the primary data to decide how many distinct  $f_0$ 's there really are.

Meantime, we would register one distinct disagreement with PDG's assignments—the placing of the lightest broad  $f_0$  at the very high mass of 1400 MeV. This is in no way to challenge the various experimental reports of  $f_0$  peaks in the 1400-MeV region; these must enter the comprehensive analysis of the higher  $f_0$  region that is now needed. The question for us is what does the  $f_0$  cross section below and just above 1 GeV correspond to spectroscopically. The answer, we would continue to assert, is a *very broad*  $f_0(1000)$  of width around 700 MeV for the following reasons.

(i) General duality notions require that the “effective position” of a meson should equal the weighted mean of the corresponding cross-section peak. Thus the twin peaks seen in the  $I=J=0$   $\pi\pi$  cross section of Fig. 1 are due to just one broad dynamical entity with the  $f_0(S^*)$  producing the dip at 1 GeV.

(ii) Analytic fits to the observed  $\pi\pi$  phase shifts from threshold to 1.4 GeV and an extensive set of other relevant reactions (the AMP analysis, [8]) yield a resonance pole at  $900 - i350$  MeV.

(iii) Finally, to get a more intuitive feel for what is going on, consider the well-known functional form of the  $I=J=0$  phase shift  $\delta_{\pi\pi}$  as a function of  $E$ . With the rapid excursion associated with the  $f_0(S^*)$  removed, this reveals a slow, steady ascent of the residual phase shift (Fig. 14) in full accord with the above interpretation and closely resembling the behavior of the corresponding  $K\pi$  channel [58].

Our guiding philosophy is that *all* resonant effects however gradual have to receive a place in spectroscopic accountancy in accord with general notions of duality. The reassertion of  $f_0(1000)$  (the  $\epsilon$  of yesteryear) obviously affects our perception of where the scalar nonet clusters in mass; the associated very large width likewise shifts our generic expectations for coupling constants. In

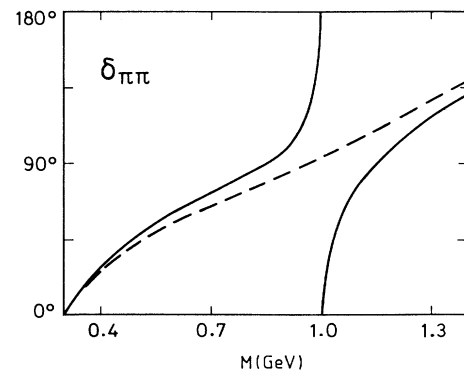


FIG. 14. Schematic representation of how, once the rapid phase movement from  $f_0(S^*)$  is removed,  $\delta_{\pi\pi}$  corresponds to a single very broad  $f_0(1000)$  resonance.

this connection, it is worth noting that the broad  $I=\frac{1}{2}$  state revealed in  $K\pi$  scattering (as mentioned above) has often been accorded a lower mass and larger width than the values listed for  $K_0^*$  (1430) in Table IV [58]. Indeed, an alternative analysis of the same experiment [58] yields a mass of 1350 MeV and width of 460 MeV.

### B. Possible spectroscopic assignments for $f_0(S^*)$

We now examine where the  $f_0(S^*)$  from our favored fit 2 solution might feature in the overall scalar picture just described. As is customary in such discussions we view possibilities in terms of stark alternatives and omit consideration of complicated mixed scenarios. We have seen that the present data disfavor a molecule interpretation for the  $f_0(S^*)$ . This leads to the obvious question: if it is not a  $K\bar{K}$  molecule, what kind of a state is it—( $q\bar{q}$ ) nonet, glueball, hybrid, or what? Given the resonance parameters that we have found, the ( $q\bar{q}$ ) nonet interpretation is not an attractive proposition; neither the rather narrow width nor the comparable couplings to  $\pi\pi$  and  $K\bar{K}$  favor such a picture. Reinstating the very broad  $f_0$  (1000) (width 700 MeV) as recommended above and identifying it as the lightest nonet member, only reinforces the argument from the width. So we are led to consider other options which divorce  $f_0(S^*)$  from the main ( $q\bar{q}$ ) spectrum. One possibility would be for  $f_0(S^*)$  to be the lightest glueball. An alternative designation could arise in Gribov's model of the QCD vacuum [55]: this assigns a special role to condensates of the light (nonstrange) quarks ( $u\bar{u}\pm d\bar{d}$ );  $f_0(S^*)$  and  $a_0(\delta)$  could be scalar excitations of this vacuum. These sharply differentiated alternatives bring out the crucial role that improved understanding of the  $a_0(\delta)$  system could play. If the  $f_0(S^*)$  is a glueball, then it is by definition dissimilar from the  $a_0(\delta)$ . Maybe this latter is *not really* narrow as several authors have argued [41,42]. This reopens the possibility of the  $a_0(\delta)$ 's being a regular ( $q\bar{q}$ ) nonet member, the  $I=1$  counterpart of the  $f_0$  (1000). In contrast, the Gribov picture would entail  $a_0(\delta)$ 's having a close resemblance to the  $f_0(S^*)$ , in fact, a state of affairs very like the  $K\bar{K}$  molecule model *except* for the range of the forces involved. These two alternatives imply very different pole structures for the  $a_0(\delta)$  which should be clearly distinguishable in an analysis such as the present one but involving the corresponding  $I=1$  decay channels. The prospects for such an analysis are now much improved as a result of data on  $\bar{p}p \rightarrow (M_1^0 M_2^0 M_3^0)$  ( $M_i^0 = \pi^0, \eta^0$  variously) acquired by the Crystal Barrel group at the CERN Low Energy Antiproton Ring (LEAR) [59]. [A capability of detecting ( $K\bar{K}\pi$ ) and ( $K\bar{K}\eta$ ) final states would greatly increase the value of these data for  $a_0(\delta)$  studies.]

Although  $a_0(\delta)$  is a prime target, any elucidation of the scalar family could bear on our understanding of the  $f_0(S^*)$ . Determining how many independent  $I=0$  scalars there really are above 1 GeV, or deciding whether  $a_0$  (1320) is a real effect, could have a major influence on our perception. Study of two-photon excitation of these sca-

lars [60] and their appearance in  $\phi$  radiative decays [61] could likewise play a vital role. Fortunately, all these areas are on the move experimentally and we can hope for significant progress on quite a short-time scale.

## VII. SUMMARY AND CONCLUSIONS

In the foregoing analysis we have investigated the resonance characteristics of the  $f_0(S^*)$  as revealed by various high statistics experiments. Our method lays stress on the strict enforcement of unitarity. This allows key new sectors of data, notably on  $J/\psi \rightarrow \phi\pi\pi(K\bar{K})$  to play their full role in refining our knowledge of the  $I=J=0$  amplitudes in the region of the  $K\bar{K}$  threshold. The principal question that we have addressed is what kind of resonance dynamics does the  $f_0(S^*)$  phenomenon manifest: is it a  $K\bar{K}$  molecule, a standard Breit-Wigner-like resonance, or, as previously suggested [8], an amalgam of two resonances? In our unitarity-enforcing framework, these possibilities translate into alternative resonance pole topologies that can be confronted with the data. The outcome of our fits is a clear preference for the standard Breit-Wigner-like description (not only is the  $\chi^2/N_{DF}$  excellent but the corresponding amplitudes are internally consistent in the nontrivial sense discussed in Sec. IV C); the alternative molecule and double resonance descriptions are rather strongly disfavored. The picture of the  $f_0(S^*)$  that emerges from our favored solution is of a somewhat narrow resonance ( $\Gamma_0 \sim 52$  MeV) with similar couplings to  $\pi\pi$  and  $K\bar{K}$ . In the previous section we describe how this might be interpreted spectroscopically and linked this to the need for a comparable analysis of the  $a_0(\delta)$  system.

As so often in meson spectroscopy, there are experimental loose ends to pursue. For  $f_0(S^*)$  and  $a_0(\delta)$  studies, all information on  $K\bar{K}$  final states, in particular that near threshold, needs strengthening. It is to be hoped that the COSY 3.3 GeV/c proton synchrotron presently being constructed at KFA-Jülich will allow the necessary high-resolution studies of  $K\bar{K}$  production to be performed [62]. The CLEO experiment [63] should shortly provide additional information on the production of scalars in two-photon reactions, while the DAΦNE project [64] will certainly enhance our knowledge of  $\phi$  radiative decays to scalars.

*Note added in proof.* Among reports of  $I=0$  scalar signals, one should mention a new amplitude analysis of peripheral dipion production by Svec *et al.* [65] which claims to reinstate the possibility of a narrow scalar resonance close to the  $\rho$  mass. Such behavior is normally excluded by examining how the  $f_0(S^*)$  effect manifests itself in  $\pi\pi$  scattering [7, 50, 66]. The new analysis needs to meet this challenge by exploring how its phase shifts extend into the  $f_0(S^*)$  region.

## ACKNOWLEDGMENTS

It is a pleasure to thank Bill Lockman, Antimo Palano, and John Weinstein for useful discussions.

- [1] For general reviews see L. Montanet, *Rep. Prog. Phys.* **46**, 337 (1983); F. E. Close, *ibid.* **51**, 833 (1988); M. R. Pennington, in *Glueballs, Hybrids and Exotic Mesons*, Proceedings of the Workshop, Upton, New York, 1988, edited by S. U. Chung, AIP Conf. Proc. No. 185 (AIP, New York, 1989), p. 145; N. Isgur, in *Hadron '89*, Proceedings of the 3rd International Conference on Hadron Spectroscopy, Ajaccio, France, 1989, edited by F. Binon *et al.* (Editions Frontières, Gif-sur-Yvette, 1989), p. 709; T. H. Burnett and S. R. Sharpe, *Annu. Rev. Nucl. Part. Sci.* **40**, 327 (1990).
- [2] D. Morgan, *Phys. Lett.* **51B**, 71 (1974); N. Törnqvist, *Phys. Rev. Lett.* **49**, 624 (1982).
- [3] R. L. Jaffe, *Phys. Rev. D* **15**, 267 (1977).
- [4] J. Weinstein and N. Isgur, *Phys. Rev. Lett.* **48**, 659 (1982); *Phys. Rev. D* **27**, 588 (1983); **41**, 2236 (1990).
- [5] R. L. Jaffe, *Phys. Lett.* **41**, 271 (1975); D. Robson, *Nucl. Phys.* **B130**, 328 (1977).
- [6] For general reviews of glueballs, hybrids, etc., see T. Barnes, in *Proceedings of the Fourth Workshop on Polarized Targets Materials and Techniques*, Bad Honnef, Germany, 1984, edited by W. Meyer (Bonn University, Bonn, 1984); J. F. Donoghue, in *Hadron Spectroscopy—1985*, Proceedings of the International Conference, College Park, Maryland, edited by S. Oneda, AIP Conf. Proc. No. 132 (AIP, New York, 1985), p. 460; see, also, Close [1].
- [7] M. Alston-Garnjost *et al.*, *Phys. Lett.* **36B**, 152 (1971).
- [8] K. L. Au, D. Morgan, and M. R. Pennington, *Phys. Rev. D* **35**, 1633 (1987).
- [9] J. P. Stroot, in *The Hadron Mass Spectrum*, Proceedings of the Conference, St. Goar, Germany, 1990, edited by E. Klempt and K. Peters [*Nucl. Phys. B (Proc. Suppl.)* **21**, 415 (1991)].
- [10] D. Aston *et al.*, *Nucl. Phys.* **B301**, 525 (1988); F. E. Close, in *Hadron '89* [1], p. 125; Montanet [1], p. 669.
- [11] D. Morgan and M. R. Pennington, *Phys. Lett. B* **258**, 444 (1991).
- [12] D. Morgan, *Nucl. Phys.* **A543**, 632 (1992).
- [13] S. Weinberg, *Phys. Rev.* **137**, B672 (1965).
- [14] L. Castillejo, R. H. Dalitz, and F. J. Dyson, *Phys. Rev.* **101**, 453 (1956).
- [15] R. E. Peierls, in *Proceedings of the 1954 Glasgow Conference on Nuclear and Meson Physics*, edited by E. H. Bellamy and R. G. Moorhouse (Pergamon, New York, 1955), p. 296; G. F. Chew, in *Old and New Problems in Elementary Particles*, edited by G. Puppi (Academic, New York, 1968), p. 80; R. H. Dalitz and R. G. Moorhouse, *Proc. R. Soc. London A* **318**, 279 (1970).
- [16] R. Jost, *Helv. Phys. Acta* **20**, 256 (1947); M. Kato, *Ann. Phys. (N.Y.)* **31**, 130 (1965). For applications along the present lines see Morgan [2]; Y. Fujii and M. Fukugita, *Nucl. Phys.* **B85**, 179 (1975); A. D. Martin, E. N. Ozmütlu, and E. J. Squires, *ibid.* **B121**, 514 (1977). For other related material see A. M. Badalyan, L. P. Kok, M. I. Polikarpov, and Yu. A. Simonov, *Phys. Rep.* **82**, 31 (1982).
- [17] R. H. Dalitz and J. G. McGinley, in *Low and Intermediate Energy Kaon-Nucleon Physics*, edited by E. Ferrari and G. Violini (Reidel, Dordrecht, Holland, 1981), p. 381; R. H. Dalitz, J. G. McGinley, C. Belyea, and S. Anthony, in *Proceedings of the Conference on Hypernuclear and Kaon Physics*, Heidelberg, Germany, 1982, edited by B. Povh (MPI, Heidelberg, 1982), p. 201.
- [18] G. C. Oades and G. Rasche, *Phys. Scr.* **26**, 15 (1982).
- [19] S. D. Protopopescu *et al.*, *Phys. Rev. D* **7**, 1279 (1973); G. Grayer *et al.*, *Nucl. Phys.* **B75**, 189 (1974); A. C. Irving, A. D. Martin, and P. J. Done, *Z. Phys. C* **10**, 45 (1981); Törnqvist [2].
- [20] Morgan [2]; Fujii and Fukugita [16]; for an alternative viewpoint based on a nonrelativistic model assuming a separable potential, see, F. Cannata, J. P. Dedonder, and L. Leśniak, *Z. Phys. A* **334**, 457 (1989); **343**, 451 (1992).
- [21] For example, Martin *et al.* [16].
- [22] A. Falvard *et al.*, *Phys. Rev. D* **38**, 2706 (1988).
- [23] U. Malik, in *Strong Interactions and Gauge Theories*, Proceedings of the XXIst Rencontre de Moriond, Les Arcs, France, 1986, edited by J. Tran Thanh Vanh (Editions Frontières, Gif-sur-Yvette, 1986), Vol. 2, p. 431; W. Lockman, in *Hadron '89* [1], p. 109; and (private communication).
- [24] G. Gidal *et al.*, *Phys. Lett.* **107B**, 153 (1981).
- [25] J. C. Anjos *et al.*, *Phys. Rev. Lett.* **62**, 125 (1989).
- [26] A. Etkin *et al.*, *Phys. Rev. D* **25**, 1786 (1982).
- [27] D. Cohen *et al.*, *Phys. Rev. D* **22**, 2595 (1980).
- [28] W. Wetzel *et al.*, *Nucl. Phys.* **B115**, 208 (1976).
- [29] V. A. Polychronakos *et al.*, *Phys. Rev. D* **19**, 1317 (1979).
- [30] R. S. Longacre *et al.*, in *Hadron '87*, Proceedings of the Second International Conference on Hadron Spectroscopy, Tsukuba, Japan, 1987, edited by Y. Oyanagi *et al.* (KEK Report No. 87-7, Tsukuba, 1987), p. 46; S. J. Lindenbaum and R. S. Longacre, *Phys. Lett. B* **274**, 492 (1992).
- [31] R. S. Longacre *et al.*, *Phys. Lett. B* **177**, 223 (1986).
- [32] T. Åkesson *et al.*, *Nucl. Phys.* **B264**, 154 (1986); P. C. Cecil, thesis, Cavendish Laboratory, Cambridge, England, Rutherford Laboratory Report No. RAL-T-004, 1984 (unpublished).
- [33] J. Carter (private communication); Cecil [32].
- [34] T. A. Armstrong *et al.*, *Z. Phys. C* **51**, 351 (1991).
- [35] Compare Irving *et al.* [19].
- [36] I. J. R. Aitchison, *Nucl. Phys.* **A189**, 417 (1972).
- [37] S. L. Adler, *Phys. Rev.* **137**, B1022 (1965); **139**, B1638 (1965).
- [38] J. Gasser and H. Leutwyler (private communication).
- [39] To be discussed in Sec. VI A below; see also Ref. [8].
- [40] For a recent application and some earlier references, see G. Dillon, *Europhys. Lett.* **20**, 389 (1992).
- [41] S. Flatté, *Phys. Lett.* **63B**, 224 (1976).
- [42] N. N. Achasov, S. A. Devyanin, and G. N. Shestakov, *Phys. Lett.* **96B**, 168 (1980).
- [43] Grayer *et al.* [19]; H. Becker *et al.*, *Nucl. Phys.* **B151**, 46 (1979).
- [44] Aston *et al.* [10].
- [45] N. M. Cason *et al.*, *Phys. Rev. D* **28**, 1586 (1983).
- [46] R. S. Longacre (private communication).
- [47] J. Weinstein (private communication, 1989).
- [48] Particle Data Group, K. Hikasa *et al.*, *Phys. Rev. D* **45**, S1 (1992).
- [49] J. Weinstein, in *Proceedings of the  $\tau$ -Charm Factory Workshop*, Stanford, California, 1989, edited by Lydia V. Beers (SLAC Report No. 343, Stanford, 1989).
- [50] Protopopescu *et al.* [19].
- [51] B. Hyams *et al.*, *Nucl. Phys.* **B64**, 134 (1973).
- [52] References for the points shown in Fig. 12 are as follows: Protopopescu '73 [50]; Hyams '73 [51]; Binnie '73—D. M. Binnie *et al.*, *Phys. Rev. Lett.* **31**, 1534 (1973); Leeper '77—R. J. Leeper *et al.*, *Phys. Rev. D* **16**, 2054 (1977); Aguilar '78—M. Aguilar-Benitez *et al.*, *Nucl. Phys.*

- B140**, 73 (1978); Gidal '81—G. Gidal *et al.* [24]; Abachi '86—S. Abachi *et al.*, Phys. Rev. Lett. **57**, 1990 (1986); Augustin '89—J. E. Augustin *et al.*, Nucl. Phys. **B320**, 1 (1989); Armstrong '91—T. A. Armstrong *et al.* [34]; Aguilar '91—M. Aguilar-Benitez *et al.*, Z. Phys. C **50**, 405 (1991). The reference for PDG '90 is Particle Data Group, J. J. Hernández *et al.*, Phys. Lett. B **239**, 1 (1990).
- [53] Evidence for this state is now reported from the Crystal Barrel experiment on  $\bar{p}p$  annihilation to  $\pi^0\eta\eta$  at LEAR, see [59].
- [54] L.-P. Chen, in *Hadron '91*, Proceedings of the International Conference on Hadron Spectroscopy, College Park, Maryland, 1991, edited by S. Oneda and D. C. Peaslee (World Scientific, Singapore, 1992), p. 111.
- [55] V. N. Gribov, Lund Report No. LU-TP-91-7, 1991 (unpublished); and (private communication).
- [56] GAMS Collaboration, M. Boutemour *et al.*, in *Hadron '89* [1], p. 119.
- [57] Aston *et al.* [10].
- [58] D. Aston *et al.*, Nucl. Phys. **B296**, 493 (1988).
- [59] Crystal Barrel Collaboration, C. Amsler *et al.*, Phys. Lett. B **291**, 347 (1992).
- [60] M. R. Pennington, in *Proceedings of Workshop on Physics and Detectors for DAΦNE*, Frascati, Italy, edited by G. Pancheri (INFN, Frascati, 1992), p. 361; D. Morgan, in *Photon-Photon '92*, Proceedings of the IXth International Workshop on Photon-Photon Collisions, San Diego, California, 1992, edited by D. O. Caldwell and H. P. Paar (World Scientific, Singapore, 1992); T. Barnes, *ibid.*, pp. 263 and 275; Z. P. Li, F. E. Close, and T. Barnes, Phys. Rev. D **43**, 2161 (1991); F. E. Close and Z. P. Li, Z. Phys. C **54**, 147 (1992).
- [61] F. E. Close, N. Isgur, and S. Kumano, Nucl. Phys. **B389**, 513 (1993).
- [62] *Proceedings of Workshop on Mesons and Mesonic States up to Slightly Above 1 GeV/c<sup>2</sup>*, edited by W. Oelert and T. Seifick (KFA, Jülich, 1991).
- [63] D. Coffman, in *Photon-Photon '92* [60].
- [64] *Proceedings of Workshop on Physics and Detectors for DAΦNE* [60].
- [65] M. Svec, A. de Lesquen, and L. van Rossum, Phys. Rev. D **46**, 949 (1992).
- [66] For background comments see note on  $f_0(1400)$  in Ref. [48], p. VII.37.